Energy Conversion and Management 157 (2018) 460–479

Contents lists available at ScienceDirect

Energy Conversion and Management

journal homepage: www.elsevier.com/locate/enconman

Parameter extraction of solar cell models using improved shuffled complex evolution algorithm

Xiankun Gao, Yan Cui*, Jianjun Hu, Guangyin Xu, Zhenfeng Wang, Jianhua Qu, Heng Wang

Key Laboratory of New Materials and Facilities for Rural Renewable Energy, Ministry of Agriculture, Henan Agricultural University, Zhengzhou 450002, China

ARTICLE INFO

Keywords:
Solar cell
Single diode model
Double diode model
Parameter extraction
Shuffled complex evolution

ABSTRACT

Fast and accurate parameter extraction of solar cell models is always desired for simulation, evaluation and maximum energy harvesting of PV systems. This paper proposes an improved shuffled complex evolution (ISCE) algorithm for parameter extraction of different PV models, including single diode model, double diode model and single diode solar module model. The novelty of proposed ISCE algorithm lies primary in the improved competitive complex evolution strategy, where three amendments are proposed to overcome the shortcomings of original SCE algorithm. (1) The expansion step and outside contraction step are inserted into to improve the probability of producing better solution. (2) The reflecting-absorbing bound- handling method is employed to enhance the chance of global search and avoid being trapped in local minima. (3) The main diagonal of simplex is adopted to overcome local roughness and drive the global search in an efficient manner. In order to test the parameter extraction performance of proposed ISCE and compare it with some state-of-the-art algorithms, the standard datasets and practical measured datasets of one solar cell and three solar modules are selected for parameter extraction of different PV models. Comparison results indicate that the proposed ISCE algorithm always exhibits the highest computational efficiency to get the most accurate parameter values among all compared algorithms. More importantly, the proposed ISCE algorithm generally promises better convergence speed and robustness than the best reported algorithms. Due to these superiorities, the proposed ISCE algorithm is quite promising and envisaged to be an accurate, efficient and reliable alternative for solving the parameter extraction problem of solar cell models.

1. Introduction

To cope with the increasing energy shortage and environment pollution, a large number of efforts have been made to accelerate energy structure adjustment and intensify the research of renewable energy. Among renewable energy technologies, solar photovoltaic is envisaged to be the most feasible candidate to meet the increasing energy demands. With the advancement of PV technology, accurate modeling and parameter extraction that closely representing the nonlinear current–voltage (*I–V*) characteristics of solar cells have drawn considerable attention in simulation, evaluation and maximum energy harvesting of PV systems [1–3]. Over the past decades, despite various models have been developed to describe the behavior of solar cells, only two lumped parameter equivalent circuit models are used practically: single diode model (SDM) and double diode model (DDM) [3–8]. There are five parameters in SDM and seven parameters in DDM need to be extracted as accurately as possible. An accurate knowledge of these parameters is of vital importance not only for performance evaluation and quality control of solar cell, but also play a important role in tracking the maximum power point (MPP) of PV systems [9–17]. Unfortunately, both SDM and DDM are implicit transcendental equations and have the shortcoming of being explicitly unsolvable using common elementary functions [18]. This inherent implicit nature hampers not only solar cell parameter extraction [19] but also PV system simulation [1]. Therefore, it is imperative to develop reliable and efficient method to accurately extract these parameters from the measured *I–V* data of solar cells.

For determining the model parameters of SDM and DDM, dozens of techniques have been developed in literature. These techniques can be generally classified into analytical methods and numerical methods. Apart from appropriate simplifying assumptions, analytical methods depend heavily upon the correctness of several key points on *I–V* curve, i.e., short-circuit current, open-circuit voltage, MPP and curve slopes at the axis intersections. Therefore, in essence, analytical methods "take a part for the whole", that is, take the selected points to generalize all measured *I–V* data. If one or more of the selected points are incorrectly assigned, the errors for the extracted parameters can be very significant

* Corresponding author.
E-mail addresses: gaoxiankun78@163.com (X. Gao), cuiyan6198@163.com (Y. Cui).

https://doi.org/10.1016/j.enconman.2017.12.033
Received 17 August 2017; Received in revised form 4 December 2017; Accepted 9 December 2017
Available online 18 December 2017
0196-8904/

Nomenclature

A	complex
B	simplex
CCE	competitive complex evolution
dim	problem dimension
D	population
DDM	double diode model
e	electronic charge ($1.60217646 \times 10^{-19}$ C)
$f_M(V, I, X)$	error function
F	objective function
g	centroid of simplex
H	smallest hypercube
I	terminal current (A)
I_0, I_{01}, I_{02}, I_{0m}	diode reverse saturation currents (A)
I_D, I_{D1}, I_{D2}	diode currents (A)
I_{ph}, I_{phm}	photocurrent (A)
IAE	individual absolute error
ISCE	improved shuffled complex evolution
k	Boltzmann constant ($1.3806503 \times 10^{-23}$ J/K)
KCL	Kirchhoff's current law
L	relative positions of simplex
LB	lower bound
m	complex size
MPP	maximum power point
Max_NFEs	maximum number of function evaluations
n, n_1, n_2, n_m	diode ideality factors
N	number of experimental I–V data
N_s	number of cells in series
N_p	the strings of cells connected in parallel
$NFEs$	number of function evaluations
p	number of complexes
P	probability or power
q	simplex size
R_s, R_{sm}	series resistance (Ω)
R_{sh}, R_{shm}	shunt resistance (Ω)
$RMSE_{cal}$	calculated root mean square error
$RMSE_{sim}$	simulated root mean square error
s	population size
SCE	shuffled complex evolution
SDM	single diode model
SMM	solar module model
thV	threshold value of RMSEcal
T	cell temperature (K)
UB	upper bound
V	terminal voltage (V)
Vth	thermal voltage (V)
x	Sample point
X	unknown parameter vector
u_d	main diagonal of simplex
u_e	extension point
u_{ic}	inside contraction point
u_{oc}	outside contraction point
u_q	the worst vertex of simplex
u_r	reflection point
u_z	random point within H
α	number of iteration for each simplex
β	number of offspring

[20]. Consequently, analytical methods are usually uncertain and offer unsatisfied results in most cases. On the contrary, numerical methods take all measured I–V data into consideration for extracting solar cell parameters at a higher confidence level. Hence, with developments in mathematics and computer science, numerical methods have prevailed in solving the problem of solar cell parameter extraction. In recent years, various deterministic methods [21–27], traditional evolutionary algorithms [28–40] and bionics evolutionary algorithms [41–59] have been applied in this field. Deterministic methods are sensitive to initial values and prone to be trapped in local minima. Although evolutionary algorithms give higher accuracy and better computational efficiency than deterministic methods, their performance depends strongly on the proper tuning of control parameters. Any improper choice can result in slow convergence and premature termination of iterations. Therefore, searching for accurate and efficient numerical algorithm to solve the problem of solar cell parameter extraction is still ongoing.

The shuffled complex evolution (SCE) is an effective and efficient global optimization algorithm developed by Duan [60] at the University of Arizona. In principle, SCE algorithm is a synthesis of four concepts that have proved successful for global optimization: controlled random search, competition evolution, complex shuffling, and the reflection step and inside contraction step of Nelder-Mead simplex algorithm [61]. The first three concepts ensure SCE algorithm flexible and robust to share the information gained independently by each complex, and thus intensify the global searching ability and avoid being trapped in local minima. As the most popular direct-search method, the deterministic Nelder-Mead simplex algorithm is powerful in local search, which can better guide the directions of global optimization. From these points of view, SCE algorithm combines the strengths of population-based stochastic evolution and deterministic direct-search to accomplish the global minimization. To sum up, the attractive features of SCE algorithm are as follows: (1) Simple to understand and easy to program; (2) Free from derivatives and lower sensitivity to initial value; (3) Powerful global search ability and high probabilistic convergence to global optimum. Given these advantages, SCE algorithm and its variants [62–66] have successfully been applied in many engineering problems, especially for hydrological model calibration. However, an exhaustive examination of the literature reveals that there is less work on the application of SCE algorithm for solving the parameter extraction problem of solar cell models. The reason behind this is that SCE algorithm has slow convergence rate when coping with the complex problems involving numerous local minima.

In light of the preceding discussion, the main contribution of this paper is to propose an improved shuffled complex evolution (ISCE) algorithm that is perfectly well capable of solving the parameter extraction problem of SDM and DDM. The main idea of proposed ISCE algorithm is to reduce the randomness and improve the probability of producing better solution, and thus to ensure the population evolving continuously toward the global optimum. To this end, three amendments are proposed to overcome the shortcomings of original SCE algorithm. The other contribution of this paper is to test the parameter extraction performance of proposed ISCE algorithm and compare it with some reported state-of-the-art algorithms. To be objective and reproducible, the standard datasets and practical measured datasets of one solar cell and three solar modules are selected for parameter extraction of different PV models. The parameter extraction results of proposed ISCE algorithm is indirectly compared with some state-of-the-art algorithms and directly compared with the best reported EHA-NMS [25] and R_{cr}-IJADE [35] algorithms in detail. Accuracy, convergence speed and robustness are chosen as the performance criteria to evaluate the parameter extraction results of them. Comparison results demonstrate that the proposed ISCE algorithm consistently exhibits better performance than reported algorithms in most cases.

The rest of this paper is organized as follows. Section 2 describes the PV models used in this work together with the objective function to be optimized for parameters extraction. Section 3 introduces the original SCE algorithm and its shortcomings. Section 4 presents the proposed ISCE algorithm in detail. Section 5 elaborates and compares the

parameter extraction results and finally, Section 6 concludes this paper.

2. Photovoltaic modeling and problem formulation

2.1. Photovoltaic modeling

From the physical perspective, a solar cell can be viewed as a large-area diode being exposed to the sunlight [67]. So for decades, the Shockley-diode based equivalent circuits have been identified as the standard way to describe the electrical behavior of solar cells. An ideal solar cell is theoretically depicted as a photocurrent source in parallel with an ideal diode. However, since no solar cell is ideal in reality, this ideal model deviates considerably from actual *I–V* characteristics. To be realistic, the non-ideal behaviors such as the effects of series and parallel parasitic losses and several conduction phenomena that significantly contribute to the current of the junction [68] should be taken into consideration for accurate modeling of solar cells. In the literature, the two most common used models are SDM and DDM detailed as below.

2.1.1. Single diode model

In the equivalent circuit of SDM illustrated by Fig. 1(a), the solar cell under illumination is modeled as a photocurrent source, a diode and two parasitic resistors. Photocurrent I_{ph} is sensitive to solar radiation and ambient temperature. The lumped series resistance R_s represents the resistance in the path of the current, including electrode resistance, contact resistance and material bulk resistance. The presence of shunt resistance R_{sh} corresponds to the leakage current across the *p-n* junction and so it is parallel to the diode. The diode D incorporates a modified diode ideality factor n to account for the combined effect of more than one type of conduction process [69] occurred within actual solar cell. It should be noted that the diode ideality factor n is a real quality index indicating how closely an actual solar cell follows the ideal solar cell, and its value depends critically upon fabrication process and semiconductor material. For a given irradiance and temperature, according to Kirchhoff's current law (KCL) and Shockley diode equation, the *I–V* relationship in Fig. 1(a) can be described by the following SDM Eq. (1).

$$I = I_{ph} - I_0\left[\exp\left(\frac{V+IR_s}{nV_{th}}\right)-1\right]-\frac{V+IR_s}{R_{sh}} \tag{1}$$

where I, V, I_{ph}, I_0, n, R_s and R_{sh} are the terminal current, terminal voltage, photocurrent, diode saturation current, diode ideality factor, series resistance and shunt resistance of a single solar cell, respectively. Thermal voltage $V_{th} = kT/e$, where $k = 1.3806503 \times 10^{-23}$ J/K is the Boltzmann constant, $e = 1.60217646 \times 10^{-19}$ C is the electronic charge, and T is the absolute temperature in Kelvin and can be calculated by 273.15 plus the cell temperature in Celsius.

From Eq. (1), it is easy to see that SDM contains five unknown parameters $\boldsymbol{X} = [I_{ph}, I_0, n, R_s, R_{sh}]$ to be extracted from the measured *I–V* data of solar cells.

2.1.2. Double diode model

In the equivalent circuit of DDM depicted in Fig. 1(b), diode D_1 simulates the diffusion process of the minority carriers into the depletion layer, while D_2 represents the carrier recombination in the space charge region of the junction [17]. Correspondingly, I_{D1} and I_{D2} stand for diffusion and recombination current components respectively. By applying KCL and Shockley diode equation, the *I–V* relationship in Fig. 1(b) can be represented as the following DDM Eq. (2).

$$I = I_{ph} - I_{01}\left[\exp\left(\frac{V+IR_s}{n_1V_{th}}\right)-1\right]-I_{02}\left[\exp\left(\frac{V+IR_s}{n_2V_{th}}\right)-1\right]-\frac{V+IR_s}{R_{sh}} \tag{2}$$

where I_{01}, I_{02}, n_1, and n_2 are the saturation currents and ideality factors of diode D_1 and D_2, respectively. The other terms are the same as those stipulated in SDM Eq. (1).

Obviously, there are seven unknown parameters $\boldsymbol{X} = [I_{ph}, I_{01}, I_{02}, n_1, n_2, R_s, R_{sh}]$ in DDM Eq. (2) to be determined from the measured *I–V* data of solar cells. It must be pointed out that DDM Eq. (2) is prone to degenerate into SDM Eq. (1). This type of model degeneration are featured by $n_1 \approx n_2 \approx n$ and $I_{01} + I_{02} = I_0$, which has been reported in our recent work [17]. Hence, there is significant sense to decrease the probability of model degeneration.

2.1.3. Single diode solar module model

It is important to note that SDM Eq. (1) and DDM Eq. (2) are characterized a single solar cell and applied at cell level. Due to its good compromise between simplicity and accuracy [70], SDM Eq. (1) has been widely used to construct the model of various PV devices. Solar module is usually assembled by connecting the identical solar cells in series and parallel configuration. Hence, SDM Eq. (1) can be directly applied to formulate the *I–V* relationship of a solar module, as shown in Eq. (3), where N_s denotes the number of cells in series while N_p represents the strings of cells connected in parallel.

$$I = I_{ph}N_p - I_0N_p\left[\exp\left(\frac{V+IR_sN_s/N_p}{nN_sV_{th}}\right)-1\right]-\frac{V+IR_sN_s/N_p}{R_{sh}N_s/N_p} \tag{3}$$

For the sake of simplicity and conciseness, Eq. (3) can be expressed as

$$I = I_{phm} - I_{0m}\left[\exp\left(\frac{V+IR_{sm}}{n_mV_{th}}\right)-1\right]-\frac{V+IR_{sm}}{R_{shm}} \tag{4}$$

where $I_{phm} = I_{ph}N_p$, $I_{0m} = I_0N_p$, $n_m = nN_s$, $R_{sm} = R_sN_s/N_p$ and $R_{shm} = R_{sh}N_s/N_p$, respectively. For brevity and definiteness, the single diode solar module model is abbreviated as SMM in this paper.

2.2. Objective function

The main objective for parameter extraction of SDM, DDM and SMM is to find a set of parameter values to minimize the errors between the calculated current and measured current, which can be formulated by an objective function. For easy comparison with the reported results of recent literature [22–59], the root mean square error (RMSE) is selected as the objective function in this paper. The optimization goal is set to

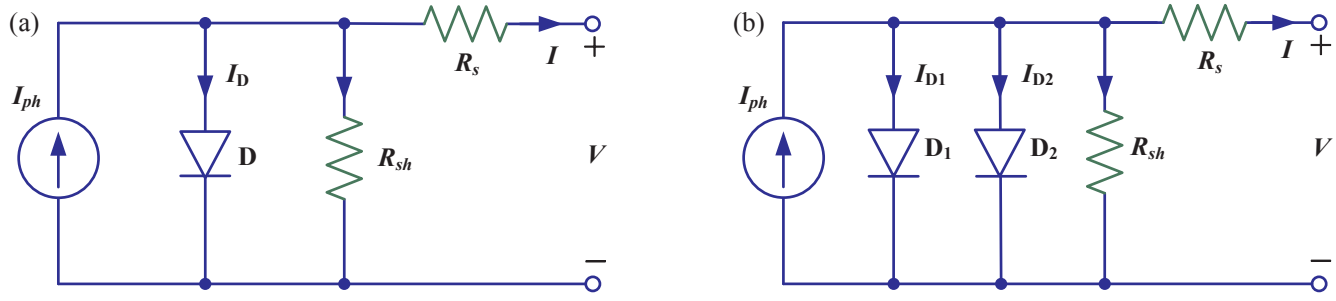

Fig. 1. Equivalent circuits of a solar cell under illumination: (a) Single diode model (SDM) and (b) Double diode model (DDM).

minimize Eq. (5) with respect to the unknown parameter vector $\boldsymbol{X}$.

$$F(\boldsymbol{X}) = RMSE_{cal}(\boldsymbol{X}) = \underset{\mathbf{x}\in[LB,UB]\in\mathbb{R}^{+}}{\text{minimize}} \sqrt{\frac{1}{N}\sum_{i=1}^{N} f_{\mathrm{M}}(V,I,\boldsymbol{X})^2} \tag{5}$$

where LB and UB are the lower and upper bounds on parameter vector $\boldsymbol{X}$, respectively. N is the number of measured I–V data. The error function $f_{\mathrm{M}}(V,I,\boldsymbol{X})$ can be formulated by Eqs. (6)(8) for SDM, DDM and SMM, respectively.

$$f_{\mathrm{SDM}}(V,I,\boldsymbol{X}) = I_{ph} - I_0\left[\exp\left(\frac{V+IR_s}{nV_{th}}\right)-1\right] - \frac{V+IR_s}{R_{sh}} - I \tag{6}$$

$$f_{\mathrm{DDM}}(V,I,\boldsymbol{X}) = I_{ph} - I_{01}\left[\exp\left(\frac{V+IR_s}{n_1V_{th}}\right)-1\right] - I_{02}\left[\exp\left(\frac{V+IR_s}{n_2V_{th}}\right)-1\right] - \frac{V+IR_s}{R_{sh}} - I \tag{7}$$

$$f_{\mathrm{SMM}}(V,I,\boldsymbol{X}) = I_{phm} - I_{0m}\left[\exp\left(\frac{V+IR_{sm}}{n_mV_{th}}\right)-1\right] - \frac{V+IR_{sm}}{R_{shm}} - I \tag{8}$$

It is evident from Eq. (5) that the smaller the RMSE_{cal} value, the more accurate the parameter values extracted from the model.

3. Shuffled complex evolution (SCE) algorithm

In this section, the main routine of original SCE algorithm, its affiliated competitive complex evolution (CCE) strategy and shortcomings are briefly discussed.

3.1. Main routine of SCE algorithm

SCE algorithm is a three-tier architecture comprising following tiers: population, complex and simplex. Hence, the philosophy behind SCE algorithm is to treat the global search as a bottom-up population evolution. To ensure the effectiveness and efficiency, SCE algorithm merges the strengths of controlled random search, competitive evolution, complex shuffling and a simplified adaptation of Nelder-Mead simplex algorithm [61] to evolve the population toward the global optimum. SCE algorithm begins with a randomly sample to constitute the initial population of points spanning the entire feasible space of [LB, UB]. Then the points of initial population are partitioned into several complexes. Each complex is independently evolved using the CCE strategy to update the worst vertex of simplex and guide the search toward improvement direction. After a certain number of generations, the updated simplex is return back to complex. Finally, the evolved complexes are forced to mix and new complexes are formed through the complex shuffling strategy to ensure the information sharing among different complexes. This evolution process is repeated until certain convergence criteria are satisfied. In this paper, we specify the maximum number of function evaluations (Max_NFEs) as the terminate criteria.

The main routine of SCE algorithm is illustrated in Fig. 2 [60] and is described below through the steps:

Step 0: Initialize: Select $p \geq 1$ and $m \geq dim + 1$, where p is the number of complexes, m is the number of points in each complex, and dim is the dimensionality of optimization problem. Compute the sample size $s = p \times m$.

Step 1: Generate sample: Sample s points $x_1, \ldots, x_s$ within [LB, UB]. Compute the function value F_i at each point x_i. In the absence of prior information, use a uniform sampling distribution. Set the number of function evaluations $NFEs = s$.

Step 2: Rank points. Sort the s points in order of increasing function value. Store them in an array $D = \{x_i, F_i, i = 1, \ldots, s\}$, so that $i = 1$ represents the point with the smallest function value.

Step 3: Partition into complexes: Partition population array D into p complexes $A^1, \ldots, A^p$, each containing m points, such that $A^k = \{x_j^k, F_j^k \mid x_j^k = x_{k+p(j-1)}, F_j^k = F_{k+p(j-1)}, j = 1,\ldots,m\}$.

Step 4: Evolve each complex. Evolve each complex A^k, $k = 1, \ldots, p$ according to the CCE strategy outlined in Section 3.2.

Step 5: Shuffle complexes. Replace $A^1, \ldots, A^p$ into D, such that $D = \{A^k, k = 1, \ldots, p\}$. Then sort D in order of increasing function value.

Step 6: Check convergence: If $NFEs >$ Max_NFEs, the convergence criteria are satisfied, stop; otherwise, return to Step 3 [60].

3.2. Competitive complex evolution (CCE) strategy

As the kernel of search and evolution, the CCE strategy is the key component of SCE algorithm. In CCE strategy, the reflection step and inside contraction step of Nelder-Mead algorithm [61] is applied to generate most of the offspring. Each new offspring is used for replacing the worst vertex of simplex and thus to evolve simplex toward the local optimum. To ensure the evolution process is competitive, a triangular probability distribution is adopted for selecting the better parents to construct the simplex. The CCE strategy required for complex evolution of SCE algorithm is illustrated in Fig. 3 and is explained as below [60].

Step 0: Initialize. Select q, α and β, where $2 \leq q \leq m$, $\alpha \geq 1$ and $\beta \geq 1$.

Step 1: Assign weights. Assign a triangular probability distribution to A^k, i.e.

$$P_i = \frac{2(m+1-i)}{m(m+1)}, \quad i = 1,\ldots,m. \tag{9}$$

The point x_1^k has the highest probability $P_1 = 2/(m+1)$, while the point x_m^k has the lowest probability $P_m = 2/[m(m+1)]$.

Step 2: Select parents. Randomly choose q distinct points $u_1, \ldots, u_q$ from A^k according to the probability distribution specified by Eq. (9). Store them in array $B = \{u_j, F_j, i = 1, \ldots, q\}$, where F_j is the function

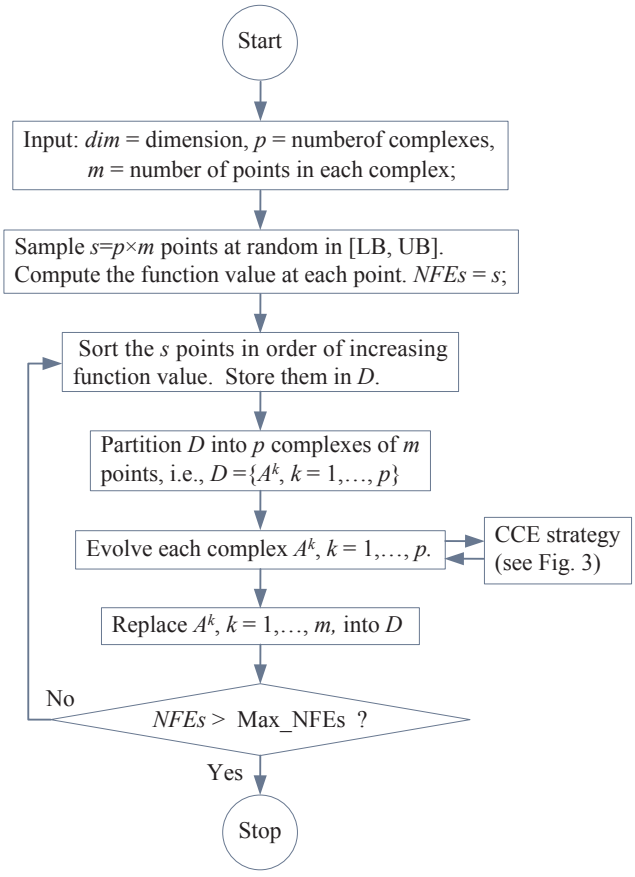

Fig. 2. Flowchart of the shuffled complex evolution (SCE) algorithm.

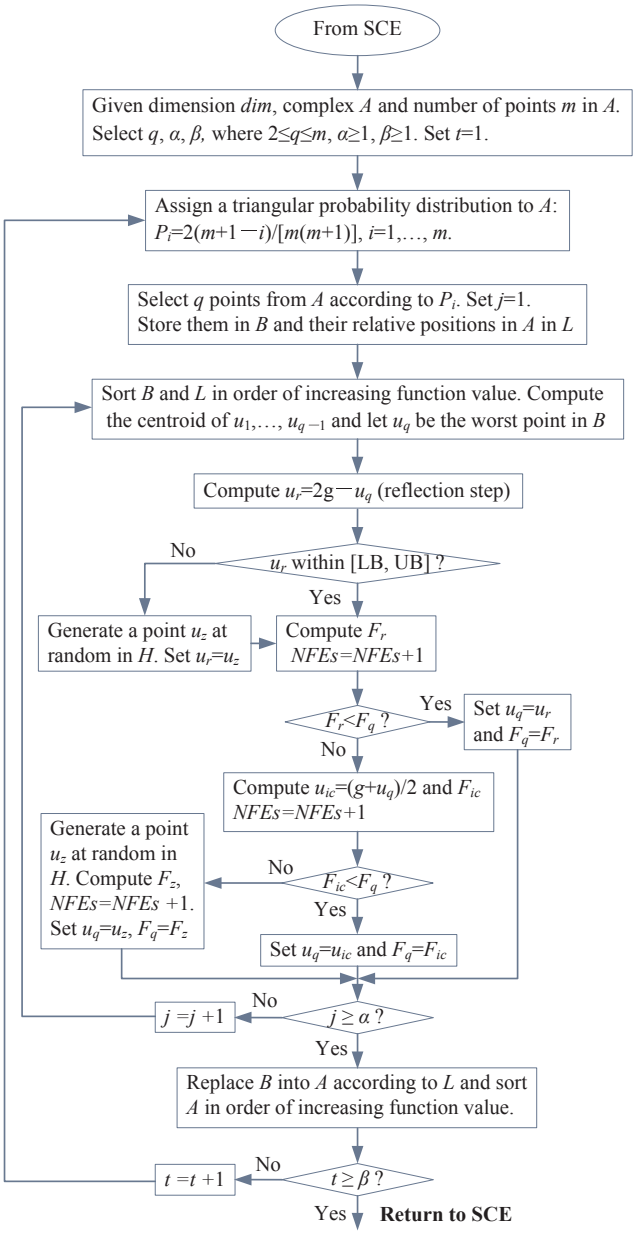

Fig. 3. Flowchart of the competitive complex evolution (CCE) strategy.

value associated with point u_j. Store in L the locations of A^k which are used to construct the simplex B.

Step 3: Generate offspring.

(a) Sort B and L so that the q points are arranged in order of increasing function value. Compute the centroid g using the expression:

$$g = \frac{1}{q-1}\sum_{j=1}^{q-1} u_j \tag{10}$$

(b) Compute the new point $u_r = 2g - u_q$ (**reflection step**).

(c) If u_r is within feasible space, compute its function value F_r and increase the number of function evaluations $NFEs = NFEs + 1$, then go to sub-step (d); else, compute the smallest hypercube H that contains A^k, randomly generate a point u_z within H, compute F_z and increase $NFEs = NFEs + 1$, set $u_r = u_z$ and $F_r = F_z$ (**mutation step**).

(d) If $F_r < F_q$, replace u_q by u_r and go to sub-step (f); else, compute $u_{ic} = (g + u_q)/2$ and its function value F_{ic}, increase $NFEs = NFEs + 1$ (**inside contraction step**).

(e) If $F_{ic} < F_q$, replace u_q by u_{ic}, go to sub-step (f); else, randomly generate a point u_z within H and compute F_z (**mutation step**), increase $NFEs = NFEs + 1$, Replace u_q by u_z.

(f) Repeat sub-steps (a) through (e) α times, where $\alpha \geq 1$ is a user-specified parameter.

Step 4: Replace parents by offspring. Replace B into A^k using the original locations stored in L. Sort A^k in order of increasing function value.

Step 5: Iterate: Repeat steps (1) through (4) β times, where $\beta \geq 1$ is a user-specified parameter which determines how many offspring should be generated.

3.3. Shortcomings of SCE algorithm

Although a large number of benchmark functions and engineering applications have proved that SCE algorithm is effective and efficient for solving global optimization problems, it still remains typically difficult to find a unique "best" parameter set, whose performance differs significantly from other parameter sets within the feasible space [LB, UB] [62]. Such poor parameter identifiability can be attributed to its slow convergence rate when coping with the complex optimization problems involving numerous local minima. The reason behind the slow convergence rate of SCE algorithm lies in three aspects. Firstly, the random mutation steps within the smallest hypercube affect its affiliated CCE strategy heavily. It is not difficult to understand that the more randomness in offspring-generating mechanism, the lower probability of producing qualified offspring [66]. Meanwhile, the reflection step and inside contraction step in CCE strategy blunder away the golden opportunity of generating better qualified offspring to keep the population being evolved. Finally, there still lacks a proper balance between the global exploration and local exploitation of SCE algorithm. As a result, SCE algorithm usually requires much more function evaluations to achieve the global optimum.

4. Improved shuffled complex evolution (ISCE) algorithm

In response to above mentioned shortcomings of original SCE algorithm, this section proposes an improved shuffled complex evolution (ISCE) algorithm to overcome them. The main routine of proposed ISCE algorithm is identical with that of original SCE algorithm. Their main difference is that the proposed ISCE algorithm evolves each complex using the improved CCE strategy proposed as follows.

4.1. Improved CCE strategy

The novelty of the improved CCE strategy is to decrease the randomness and enhance the probability of producing better qualified offspring and thus to ensure the population evolving continuously toward the global optimum. The flowchart of the improved CCE strategy is illustrated in Fig. 4. It is clear from Fig. 4 that most steps of improved CCE strategy are identical with that of original CCE strategy, except the Step 3, which is amended through the following sub-steps:

Step 3: Generate offspring.

(a) Sort B and L so that the q points are ranked in order of increasing function value. Correspondingly, u_1, u_{q-1} and u_q are respectively the best vertex, the second worst vertex and the worst vertex in simplex B. Compute the centroid g using Eq. (10).

(b) **Reflection:** Reflect the worst point u_q around g to create the reflection point $u_r = 2g - u_q$. Then handle the boundary constraints on u_r, compute its function value F_r and increase the number of function evaluations $NFEs = NFEs + 1$. If $F_1 \leq F_r < F_{q-1}$, replace u_q with u_r, F_q with F_r and go to sub-step (g).

(c) **Expansion:** If $F_r < F_1$, reflect g around u_r to get the extension point

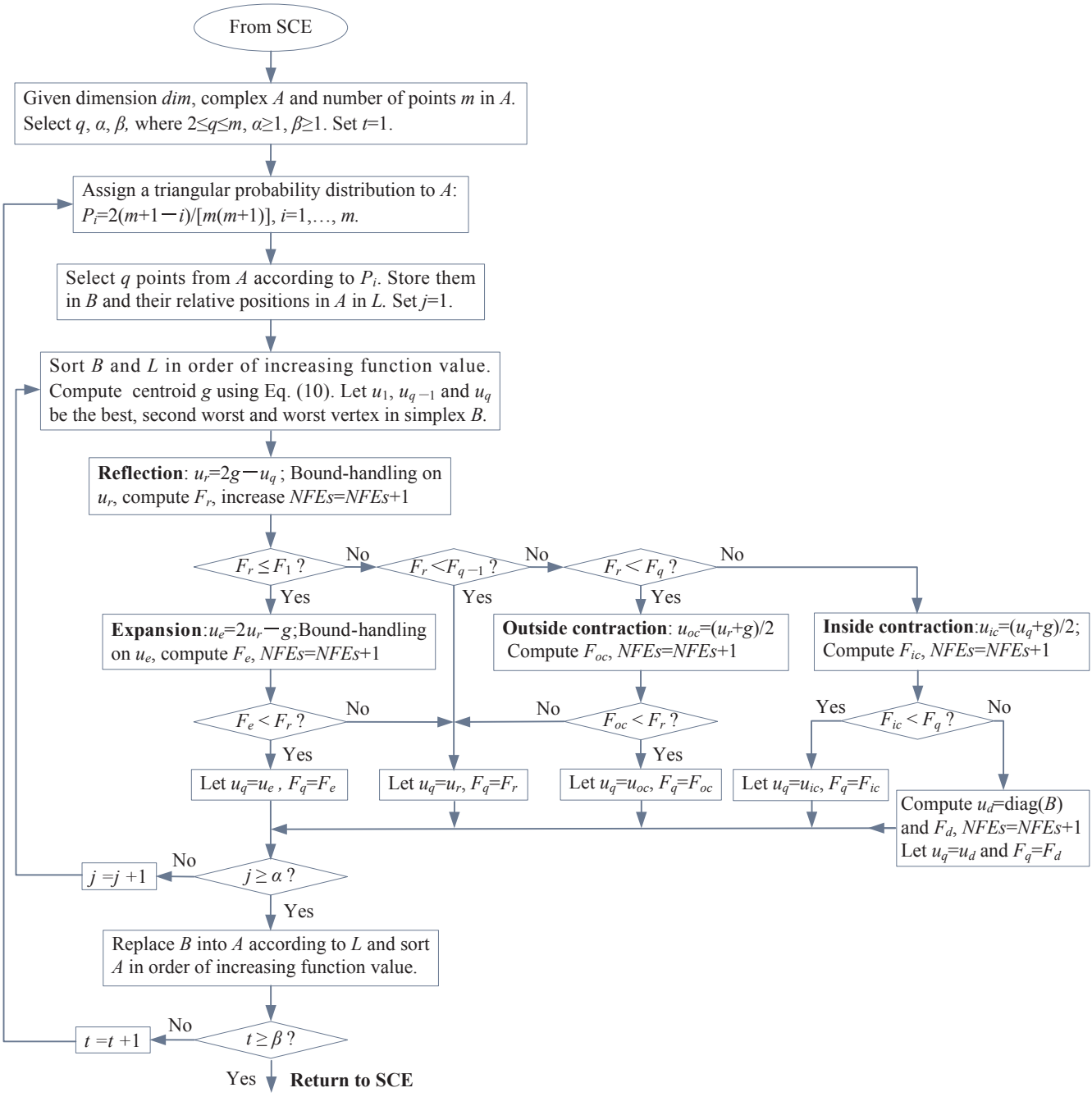

Fig. 4. Flowchart of the improved competitive complex evolution strategy.

$u_e = 2u_r - g$. Then handle the boundary constraints on u_e, compute F_e and increase $NFEs = NFEs + 1$. If $F_e < F_r$, replace u_q with u_e, F_q with F_e and go to sub-step (g). Otherwise, replace u_q with u_r, F_q with F_r and go to sub-step (g).

(d) **Outside contraction:** If $F_{q-1} \le F_r < F_q$, compute outside contraction point $u_{oc} = (u_r + g)/2$. Compute F_{oc} and increase $NFEs = NFEs + 1$. If $F_{oc} < F_r$, replace u_q with u_{oc}, F_q with F_{oc} and go to sub-step (g). Otherwise, replace u_q with u_r, F_q with F_r and go to sub-step (g).

(e) **Inside contraction:** If $F_q \le F_r$, compute inside contraction point $u_{ic} = (u_q + g)/2$. Compute F_{ic} and increase $NFEs = NFEs + 1$. If $F_{ic} < F_q$, replace u_q with u_{ic}, F_q with F_{ic} and go to sub-step (g).

(f) Otherwise, get the main diagonal of simplex B using Eq. (11), compute its function value F_d and increase $NFEs = NFEs + 1$. Then replace u_q with u_d, F_q with F_d and go to sub-step (g).

$$u_d = diag(B) \tag{11}$$

(g) Repeat sub-steps (a) through (f) α times, where $\alpha \ge 1$ is a user-specified parameter.

As can be seen from above that, three amendments are implemented in the improved CCE strategy to enhance the evolution efficiency, including: (1) The expansion step and outside contraction step are inserted between reflection step and inside contraction step to improve the probability of generating better qualified offspring; (2) The random mutation steps within the smallest hypercube of original CCE strategy are removed and replaced with the reflecting -absorbing bound-handling method; (3) The main diagonal of simplex B is used to replace the worst vertex when inside contraction step failed to produce qualified offspring. The theoretical supports for these amendments are explained

briefly as below.

As shown in Fig. 4, the intervention of expansion step and outside contraction step subdivide the feasible parameter sets into several subdomains. This makes it possible to pick more accurate offspring to replace the worst vertex of simplex. The extension point u_e and outside contraction point u_{oc} are undoubtedly better qualified than reflection point u_r for updating the simplex toward local optimum.

According to the research of [71], the bound-handling scheme is critical to the performance of particle swarm optimizer. This phenomenon has also been observed in SCE algorithm. In original CCE strategy, the mutation steps generate offspring by the random bound-handling method. Even more regrettably, these offspring are produced within the smallest hypercube H rather than the entire feasible space of [LB, UB], which further decreases the probability of generating better qualified offspring. In our improved CCE strategy, the reflecting-absorbing bound-handling method is formulated by Eq. (12), where $k = 1, \ldots, dim$ and dim is the dimension of optimization problem. Once the element of reflection point u_r or extension point u_e is outside the feasible space [LB, UB], the first two lines of Eq. (12) act like a mirror to reflect the projection of element's displacement [71]. For the oversize element, the last line of Eq. (12) relocates it at the boundary LB or UB. Hence, the reflecting-absorbing bound- handling method can effectively avoid the restriction of being evolved within subspace and enhances the chance of global search.

$$\begin{cases} u(u > UB) = 2\mathrm{UB}(u > UB) - u(u > UB) \\ u(u < \mathrm{LB}) = 2\mathrm{LB}(u < \mathrm{LB}) - u(u < \mathrm{LB}) \\ u(k) = max\{LB(k), min[UB(k), u(k)]\} \end{cases} \quad (12)$$

According to Nelder-Mead simplex algorithm [61], a shrinkage transformation should be performed when outside step and inside contraction step failed to produce qualified offspring. However, the shrinkage transformation requires dim function evaluations and there is no guarantee that its new offspring are more accurate than the worst vertex. Moreover, since outside contraction and inside contraction steps do not often fail, the shrink transformation is rare in practice [61]. Furthermore, the research of [66] discerns that shrinkage transformation jeopardizes the ability of escaping from local minima, despite it can largely increase the convergence rate. In this context, we excluded the shrinkage transformation from our improved CCE strategy and adopt the reflection point u_r to replace the worst vertex u_q when outside contraction step failed, mainly because the function values at which satisfy $F_r < F_q$ and there is no further function evaluation needed. If the inside contraction step failed to generate qualified offspring, the worst vertex u_q will be replaced with a point u_d representing the main diagonal of simplex B, regardless of the function value at it. This operation is similar to the inverse process of creating the initial simplex [61], which has the strength of overcoming local roughness and can drive the evolution in an efficient manner. In our experience, the function value at u_d has a great chance to be more accurate than the worst vertex u_q. Therefore, replacing u_q with u_d is reasonable and valid for producing qualified offspring, and thus can exclude the randomness of mutation steps in original CCE strategy.

4.2. Application setting of ISCE algorithm

4.2.1. Tuning parameters

Just like other stochastic evolution algorithms, the proposed ISCE algorithm has some tuning parameters to be selected for different problems. One can see from Figs. 2 and 4 that there are five tuning parameters in the proposed ISCE algorithm, including the number of complexes p, the size of each complex m, the size of each simplex q, the number of offspring β and the number of iteration for each simplex α. In the main routine of proposed ISCE algorithm, increasing the population size $s = p \times m$ will increase the opportunity of finding the promising regions of global optima, but it will drag down the evolution efficiency [66]. Within the improved CCE strategy, the simplex size q is subjected to the Nelder-Mead simplex [61] and assigned with $dim + 1$. As for the other two tuning parameters, increasing the number of simplex iteration $\alpha \times \beta$ will increase the convergence rate and the likelihood of being trapped in local minima.

Hence, it is very important to maintain a proper balance between the global exploration and local exploitation of proposed ISCE algorithm. According to the suggestions of [60] and for the interest of solar cell parameter extraction, the tuning parameters of proposed ISCE algorithm are consistently chosen to be Eq. (13) for parameter extraction of SDM and SMM, and Eq. (14) for parameter extraction of DDM in this paper.

$$p = dim-3,\ m = 2dim + 1,\ q = dim + 1,\ \beta = dim + 1,\ \alpha = 1 \quad (13)$$

$$p = dim-3,\ m = dim + 1,\ q = dim + 1,\ \beta = dim + 1,\ \alpha = 1 \quad (14)$$

4.2.2. Terminate criteria

Since the tuning parameter values in Eqs. (13) and (14) are kept as default in parameter extraction of SDM, DDM and SMM, only the terminate criteria of proposed ISCE algorithm need to be given by the user. In order to compare with the reported results in recent literature, the maximum number of function evaluations (Max_NFEs) is chosen as the terminate criteria of proposed ISCE algorithm, as shown in Fig. 2. Note that the number of function evaluations (*NFEs*) in Figs. 2 and 4 is a good indicator of computational efficiency, mainly because it is independent of the computer and software platform used [72]. In this paper, the proposed ISCE algorithm is coded in Matlab.

Moreover, in order to decrease the probability of DDM Eq. (2) degenerates into SDM Eq. (1), an additional constraint that the diode ideality factors n_1 and n_2 satisfy $\mathrm{abs}(n_2/n_1 - 1) > 0.15$ is imposed in parameter extraction of DDM. After the sub-step (g) of improve CEE strategy, if $NFEs <$ Max_NFEs/5 and the constraint is not satisfied for certain vertex of simplex, the main diagonal of remaining vertex is adopted to replace the unsatisfied vertex.

4.3. Difference between ISCE and existing works

Recently several variants [62–66] of SCE algorithm have been developed for scientific researches and engineering applications. Therefore, it is necessary to clarify the difference between the proposed ISCE algorithm and existing works. Authors in [62] reported a shuffled

Table 1
Lower bound (LB) and upper bound (UB) on model parameters of the four solar cell/modules.

Parameters	R.T.C. France solar cell		Parameters	Photowatt-PWP201 module		STM6-40/36 module		STP6-120/36 module	
Search ranges	LB	UB	Search ranges	LB	UB	LB	UB	LB	UB
I_{ph} (A)	0	1	I_{phm} (A)	0	2	0	2	0	8
I_0, I_{01}, I_{02} (μA)	0	1	I_{0m} (μA)	0	50	0	50	0	50
n, n_1, n_2	1	2	n_m	1	50	1	60	1	50
R_s (Ω)	0	0.5	R_{sm} (Ω)	0	2	0	0.36	0	0.36
R_{sh} (Ω)	0	100	R_{shm} (Ω)	0	2000	0	1000	0	1500

Table 2
Comparison among various parameter extraction algorithms for single diode model of R.T.C. France solar cell.

Algorithms	I_{ph} (A)	I_0 (μA)	n	R_s (Ω)	R_{sh} (Ω)	RMSE$_{cal}$	NFEs
ISCE	0.76077553	0.32302083	1.48118360	0.03637709	53.71852771	**9.860219E−04**	**5000**
EHA-NMS [25]	0.76077553	0.32302080	1.48118359	0.03637709	53.71852139	**9.860219E−04**	**5000**
R_{cr}-IJADE [35]	0.76077553	0.32302080	1.48118360	0.03637709	53.71852500	9.860219E−04	10000
PCE [38]	0.760776	0.323021	1.481074	0.036377	53.718525	9.86022E−04	10000
ABC [46]	0.7608	0.3251	1.4817	0.0364	53.6433	9.8620E−04	10000
GOTLBO [42]	0.760780	0.331552	1.483820	0.036265	54.115426	9.87442E−04	10000
CSO [53]	0.76078	0.3230	1.48118	0.03638	53.7185	9.8602E−04	15000
STLBO [43]	0.76078	0.32302	1.48114	0.03638	53.7187	9.8602E−04	50000
ABC-DE [31]	0.76077	0.32302	1.47986	0.03637	53.7185	9.8602E−04	120000
BMO [52]	0.76077	0.32479	1.48173	0.03636	53.8716	9.8608E−04	150000
NM-MPSO [26]	0.76078	0.32306	1.48120	0.03638	53.7222	9.8602E−04	350000
MABC [47]	0.760779	0.321323	1.481385	0.036389	53.39999	9.8610E−04	60000
GGHS [41]	0.76092	0.32620	1.48217	0.03631	53.0647	9.9097E−04	150000
ABSO [51]	0.76080	0.30623	1.47583	0.03659	52.2903	9.9124E−04	150000
IGHS [41]	0.76077	0.34351	1.48740	0.03613	53.2845	9.9306E−04	150000
CPSO [29]	0.7607	0.4000	1.5033	0.0354	59.012	1.3900E−03	45000
CWOA [56]	0.76077	0.3239	1.4812	0.03636	53.7987	9.8602E−04	1500000

Table 3
Simulated results of ISCE algorithm for single diode model of R.T.C. France solar cell.

Item	Measured data		Simulated current data		Simulated power data	
	V (V)	I (A)	I_{sim} (A)	IAE_{sim} (A)	P_{sim} (W)	IAE_{sim} (W)
1	−0.2057	0.7640	0.76408764	0.00008764	−0.15717283	0.00001803
2	−0.1291	0.7620	0.76266264	0.00066264	−0.09845975	0.00008555
3	−0.0588	0.7605	0.76135473	0.00085473	−0.04476766	0.00005026
4	0.0057	0.7605	0.76015423	0.00034577	0.00433288	0.00000197
5	0.0646	0.7600	0.75905585	0.00094415	0.04903501	0.00006099
6	0.1185	0.7590	0.75804301	0.00095699	0.08982810	0.00011340
7	0.1678	0.7570	0.75709159	0.00009159	0.12703997	0.00001537
8	0.2132	0.7570	0.75614207	0.00085793	0.16120949	0.00018291
9	0.2545	0.7555	0.75508732	0.00041268	0.19216972	0.00010503
10	0.2924	0.7540	0.75366447	0.00033553	0.22037149	0.00009811
11	0.3269	0.7505	0.75138806	0.00088806	0.24562876	0.00029031
12	0.3585	0.7465	0.74734834	0.00084834	0.26792438	0.00030413
13	0.3873	0.7385	0.74009688	0.00159688	0.28663952	0.00061847
14	0.4137	0.7280	0.72739678	0.00060322	0.30092405	0.00024955
15	0.4373	0.7065	0.70695327	0.00045327	0.30915067	0.00019822
16	0.4590	0.6755	0.67529489	0.00020511	0.30996036	0.00009414
17	0.4784	0.6320	0.63088431	0.00111569	0.30181505	0.00053375
18	0.4960	0.5730	0.57208207	0.00091793	0.28375271	0.00045529
19	0.5119	0.4990	0.49949164	0.00049164	0.25568977	0.00025167
20	0.5265	0.4130	0.41349356	0.00049356	0.21770436	0.00025986
21	0.5398	0.3165	0.31721950	0.00071950	0.17123509	0.00038839
22	0.5521	0.2120	0.21210317	0.00010317	0.11710216	0.00005696
23	0.5633	0.1035	0.10272135	0.00077865	0.05786294	0.00043861
24	0.5736	−0.0100	−0.00924885	0.00075115	−0.00530514	0.00043086
25	0.5833	−0.1230	−0.12438136	0.00138136	−0.07255165	0.00080575
26	0.5900	−0.2100	−0.20919308	0.00080692	−0.12342392	0.00047608
Sum of IAE_{sim}				0.01770412		0.00658366
RMSE$_{sim}$				7.75391251E−04		3.27099637E−04

complex evolution metropolis algorithm adopting the sequence evolution metropolis strategy to produce new offspring. A differential evolution based and a pattern search based shuffled complex evolution approaches are developed in [63] and [64], respectively. These hybrid algorithms are fundamentally different from the proposed ISCE algorithm. An improved shuffled complex evolution algorithm with sequence mapping mechanism is reported in [65], where a random variable $t \in (0, 1)$ is used to adjust the reflection step and inside contraction step in an attempt to make the new offspring closer to the best vertex of simplex. It is conceivable that this adaptation increases the randomness of generating qualified offspring, which is exactly contradictory to the idea of our improved CCE strategy.

In literature, the most similar case to our improved CCE strategy is the MCCE strategy reported in [66]. However, there are two differences between of them. In the MCCE strategy of [66], the first point of complex is excluded to be assigned a triangular probability and is always included in simplex to produce qualified offspring. In contrast, our improved CCE strategy assigns a triangular probability to each point of complex and the first point is not always included in simplex for generating qualified offspring. More importantly, the MCCE strategy of [66] employs the complicated random multi-normal sampling while our improved CCE strategy adopts the simple main diagonal of simplex to replace the worst vertex. This further makes our proposed ISCE algorithm free from population dimensionality monitoring and restoration used in [66]. For these reasons, our proposed ISCE algorithm is significantly different from the SP-UCI algorithm in [66].

5. Parameter extraction results and discussion

In this section, the performance of proposed ISCE algorithm is

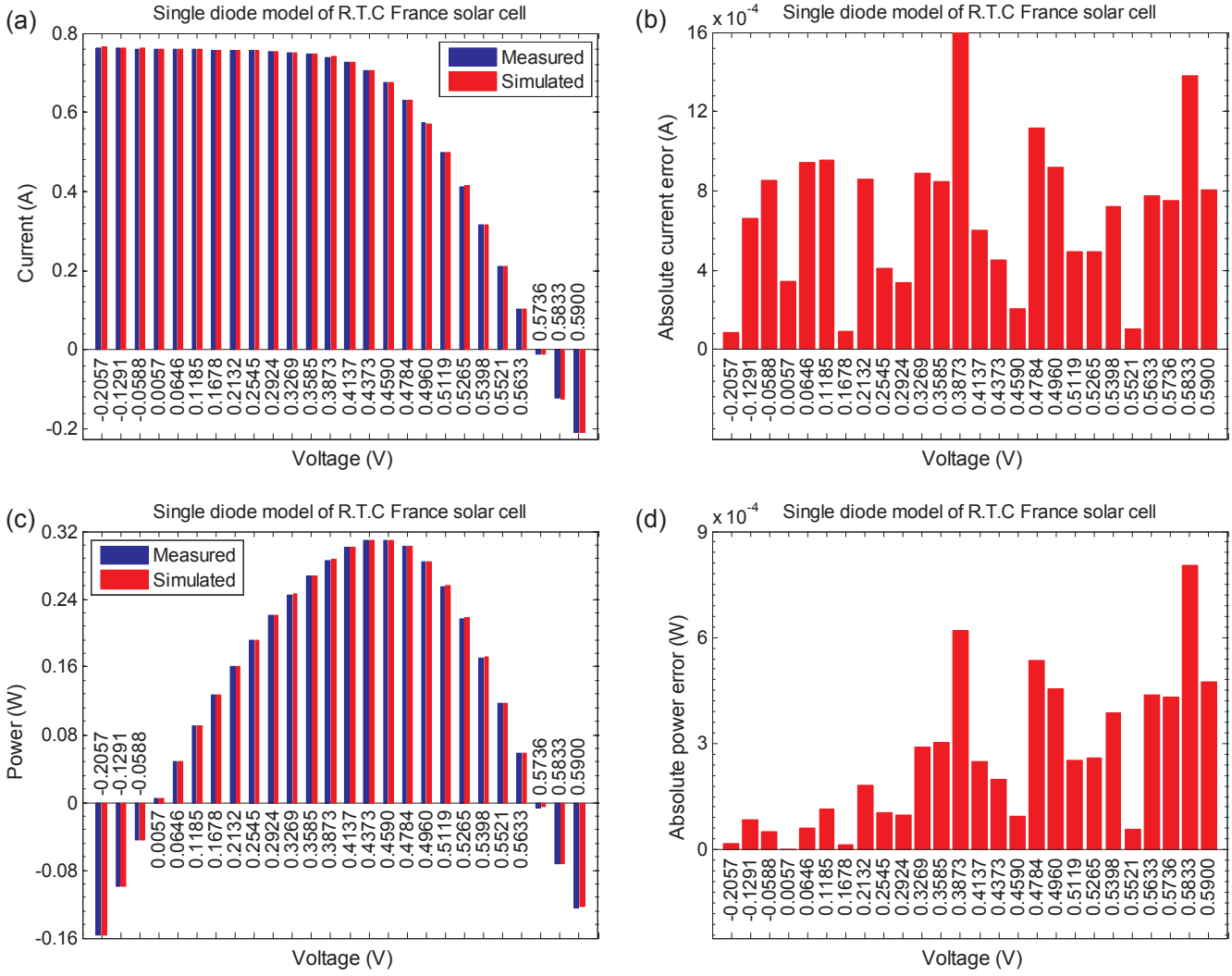

Fig. 5. Comparison between the measured data and the simulated data obtained by ISCE algorithm for single diode model of R.T.C. France solar cell: (a) *I–V* data, (b) Absolute current error, (c) *P–V* data and (d) Absolute power error.

Table 4
Comparison among various parameter extraction algorithms for double diode model of R.T.C. France solar cell.

Algorithms	I_{ph} (A)	I_{01} (μA)	I_{02} (μA)	n_1	n_2	R_s (Ω)	R_{sh} (Ω)	RMSE$_{cal}$	NFEs
ISCE	0.76078108	0.22597409	0.74934898	1.45101670	2.000000	0.03674043	55.48544409	**9.824849E−04**	**10000**
EHA-NMS [25]	0.76078108	0.22597420	0.74934836	1.45101674	2.000000	0.03674043	55.48544722	**9.824849E−04**	**10000**
R$_{cr}$-IJADE [35]	0.76078108	0.22597414	0.74934851	1.45101670	2.000000	0.03674043	55.48543800	9.824849E−04	20000
PCE [38]	0.760781	0.226015	0.749340	1.450923	2.000000	0.03674	55.483160	9.8248E−04	20000
CSO [53]	0.76078	0.22732	0.72785	1.45151	1.99769	0.036737	55.3813	9.8252E−04	15000
GOTLBO [42]	0.760752	0.800195	0.220462	1.999973	1.448974	0.036783	56.075304	9.83177E−04	20000
STLBO [43]	0.76078	0.22566	0.75217	1.45085	2.00000	0.03674	55.4920	9.8248E−04	50000
ABCDE [31]	0.76078	0.22599	0.75437	1.44972	1.99998	0.03674	55.4921	9.8246E−04	120000
MABC [47]	0.7607821	0.24102992	0.6306922	1.4568573	2.0000538	0.03671215	54.7550094	9.8276 E−04	120000
BMO [52]	0.76078	0.21110	0.87688	1.44533	1.99997	0.03682	55.8081	9.8262E−04	150000
ABSO [51]	0.76078	0.26713	0.38191	1.46512	1.98152	0.03657	54.6219	9.8344E−04	150000
IGHS [41]	0.76079	0.97310	0.16791	1.92126	1.42814	0.03690	56.8368	9.8635E−04	150000
GGHS [41]	0.76056	0.37014	0.13504	1.49638	1.92998	0.03562	62.7899	1.0684E−03	150000
NM-MPSO [26]	0.76078	0.22476	0.75524	1.45054	1.99998	0.03675	55.5296	9.8250E−04	350000
ABC [46]	0.7608	0.0407	0.2847	1.4495	1.4885	0.0364	53.7804	9.861E−04	1500000
CWOA [56]	0.76077	0.24150	0.60000	1.45651	1.9899	0.03666	55.2016	9.8272E−04	1500000

evaluated for parameter extraction of SDM, DDM and SMM of various solar cell/modules. For comparing with the reported results in recent literature, the standard datasets of a benchmark solar cell and a benchmark solar module are selected. The standard datasets are taken from [21], where the measurements are carried out on a 57 mm diameter commercial silicon R.T.C. France solar cell at 33 °C and a Photowatt-PWP201 module comprising 36 polycrystalline silicon cells in series at 45 °C. These two sets of measured *I–V* data are very representative, because they have been extensively adopted in literature as the benchmarks to test and compare the performance of various

Table 5
Simulated results of ISCE algorithm for double diode model of R.T.C. France solar cell.

Item	Measured data		Simulated current data		Simulated power data	
	V (V)	I (A)	I_{sim} (A)	IAE_{sim} (A)	P_{sim} (W)	IAE_{sim} (W)
1	−0.2057	0.7640	0.76398342	0.00001658	−0.15715139	0.00000341
2	−0.1291	0.7620	0.76260370	0.00060370	−0.09845214	0.00007794
3	−0.0588	0.7605	0.76133714	0.00083714	−0.04476662	0.00004922
4	0.0057	0.7605	0.76017400	0.00032600	0.00433299	0.00000186
5	0.0646	0.7600	0.75910828	0.00089172	0.04903839	0.00005761
6	0.1185	0.7590	0.75812202	0.00087798	0.08983746	0.00010404
7	0.1678	0.7570	0.75718848	0.00018848	0.12705623	0.00003163
8	0.2132	0.7570	0.75624423	0.00075577	0.16123127	0.00016113
9	0.2545	0.7555	0.75517766	0.00032234	0.19219271	0.00008204
10	0.2924	0.7540	0.75372286	0.00027714	0.22038856	0.00008104
11	0.3269	0.7505	0.75139611	0.00089611	0.24563139	0.00029294
12	0.3585	0.7465	0.74729616	0.00079616	0.26790567	0.00028542
13	0.3873	0.7385	0.73999138	0.00149138	0.28659866	0.00057761
14	0.4137	0.7280	0.72726488	0.00073512	0.30086948	0.00030412
15	0.4373	0.7065	0.70683581	0.00033581	0.30909930	0.00014685
16	0.4590	0.6755	0.67523011	0.00026989	0.30993062	0.00012388
17	0.4784	0.6320	0.63088763	0.00111237	0.30181664	0.00053216
18	0.4960	0.5730	0.57214027	0.00085973	0.28378157	0.00042643
19	0.5119	0.4990	0.49957059	0.00057059	0.25573018	0.00029208
20	0.5265	0.4130	0.41355632	0.00055632	0.21773740	0.00029290
21	0.5398	0.3165	0.31724207	0.00074207	0.17124727	0.00040057
22	0.5521	0.2120	0.21208148	0.00008148	0.11709018	0.00004498
23	0.5633	0.1035	0.10267156	0.00082844	0.05783489	0.00046666
24	0.5736	−0.0100	−0.00929723	0.00070277	−0.00533289	0.00040311
25	0.5833	−0.1230	−0.12439038	0.00139038	−0.07255691	0.00081101
26	0.5900	−0.2100	−0.20914692	0.00085308	−0.12339668	0.00050332
Sum of IAE_{sim}				0.01731854		0.00655394
$RMSE_{sim}$				7.57585371E−04		3.27177602E−04

algorithms [22–59] for parameter extraction of SDM, DDM and SMM. In order to further verify the effectiveness of proposed ISCE algorithm and to be objective and reproducible, the practical measured *I–V* datasets of two recent reported solar modules are also selected for parameter extraction. The practical measured *I–V* datasets are gotten from [73], where a simple load scanning experiment was set up to measure the *I–V* data of two solar modules: mono-crystalline STM6-40/36 and polycrystalline STP6-120/36. Both solar modules contain 36 cells in series, while operating at 51 °C and 55 °C, respectively.

In order to manifest the superior performance of proposed ISCE algorithm, its accuracy is firstly compared with the reported results in recent literature with respect to $RMSE_{cal}$ value and extracted parameter values. Then, the convergence and robustness of proposed ISCE are directly compared with the best reported EHA-NMS [25] and R_{cr}-IJADE [35] algorithms. To ensure a fair comparison, the searching ranges were maintained in the parameter extraction process of proposed ISCE, EHA-NMS and R_{cr}-IJADE algorithms. The search ranges for standard datasets of R.T.C. France solar cell and Photowatt-PWP201 module [21] are set the same as [22–59] and given in Table 1. According the well extracted parameter values reported in [73] and similar to the parameter boundary of standard datasets, the search ranges for the practical measured *I–V* datasets of STM6-40/36 and STP6-120/36 modules [73] are set as Table 1. The terminate criteria of proposed ISCE algorithm is set to be Max_NFEs = 5000 for parameter extraction of SDM and SMM, and Max_NFEs = 10,000 for parameter extraction of DDM, which are identical to those of EHA-NMS [25] algorithm but only half those of R_{cr}-IJADE algorithm [35]. Furthermore, in order to achieve a higher confidence level of comparison results, 1000 independent runs of proposed ISCE, EHA-NMS and R_{cr}-IJADE algorithms are implemented for parameter extraction of SDM, DDM and SMM of the four solar cell/modules. The proposed ISCE and EHA-NMS [25] algorithms are implemented in Matlab 2016b, while R_{cr}-IJADE [35] algorithm is executed in Visual Studio 2013. All comparative experiments were executed on a personal laptop with an Intel Core i5 4300M processor @ 2.60 GHz, 4 GB RAM, under the Windows 7 64-bit OS.

5.1. Results on standard datasets

5.1.1. Accuracy for single diode model

For the single diode model of R.T.C. France solar cell at 33 °C [21], the parameter extraction results of proposed ISCE algorithm are compared with the reported results of some recent algorithms listed in Table 2. The reason for selecting these algorithms for comparison is due to their good performance and the maximum number of function evaluations of them is available in the literature. The parameter extraction results used for accuracy comparison include the $RMSE_{cal}$ value and corresponding parameter values. The overall best performance among the compared algorithms is highlighted in bold.

One can see from Table 2 that the proposed ISCE algorithm, together with the EHA-NMS, R_{cr}-IJADE, PCE, CSO, STLBO, ABC-DE, and NM-MPSO algorithms acquire the optimal $RMSE_{cal}$ value, although they have different significant digits. Moreover, as can be seen from Table 2 that the proposed ISCE algorithm and EHA-NMS algorithm require the least number of function evaluations to get the optimal $RMSE_{cal}$ value among all compared algorithms. This means these two algorithms have the highest computational efficiency to get the most accurate parameter values of single diode model.

To verify the accuracy of optimal parameter values extracted by ISCE algorithm, they are back-substituted into Eq. (1) to reconstruct the simulated current data and simulated power data at measured voltage point. As we have mentioned in [17], this is simply done by using the *fzero* function or bisection method [25] or Newton method [51] when *V* is known while *I* is unknown. The simulated data and the individual absolute error (IAE) between measured and simulated data are enlisted in Table 3 and illustrated in Fig. 5, respectively.

One can see from Fig. 5(a) and (c) that the simulated *I–V* data and *P–V* data are in well agreement with the measured data for the single diode model of R.T.C. France solar cell. Fig. 5(b and d) and the next-to-last line of Table 3 indicate that the IAE_{sim} and their sum is negligible small. These give concrete evidence that the parameter values extracted by ISCE algorithm are very accurate.

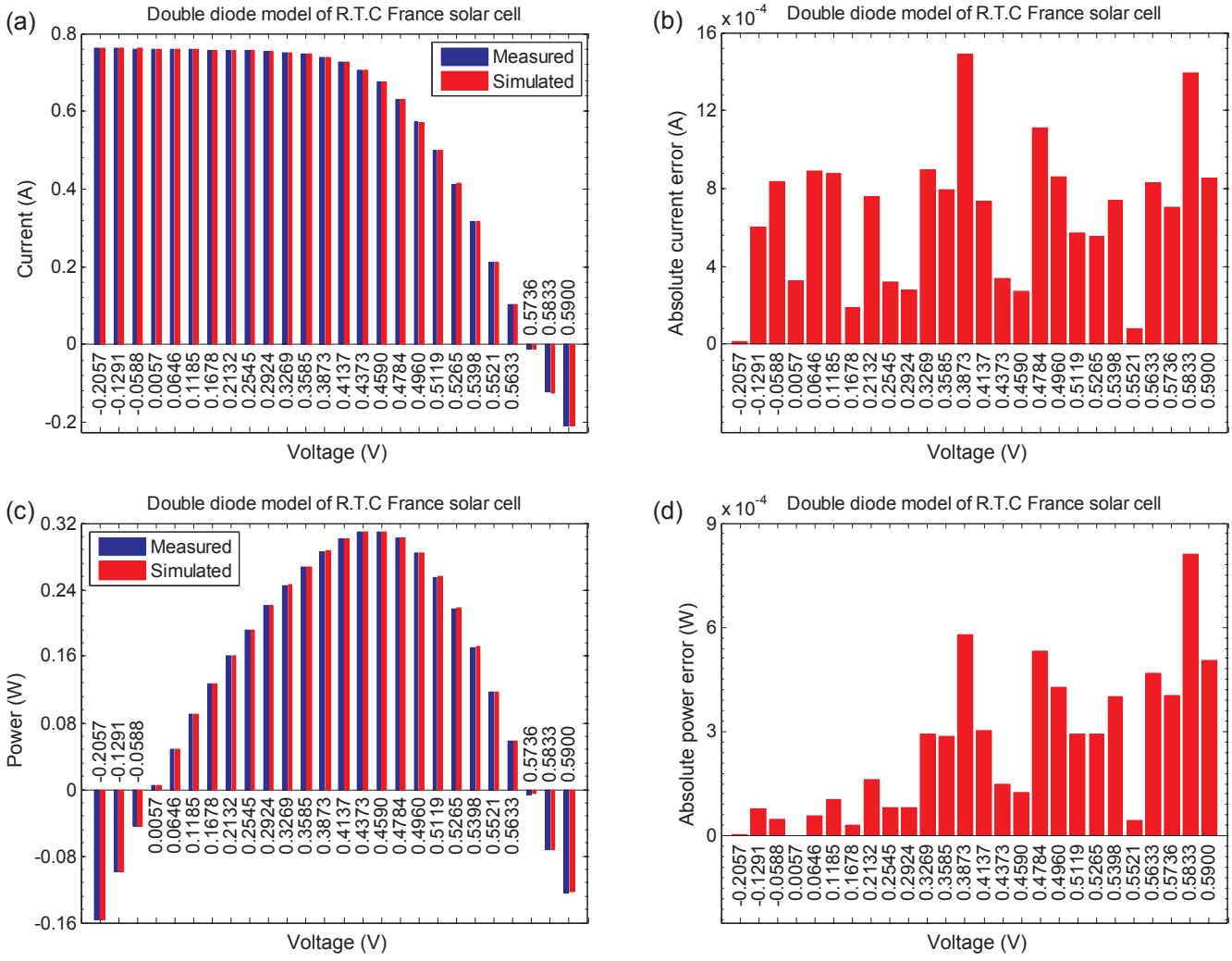

Fig. 6. Comparison between the measured data and the simulated data obtained by ISCE algorithm for double diode model of R.T.C. France solar cell: (a) *I–V* data, (b) Absolute current error, (c) *P–V* data and (d) Absolute power error.

Table 6
Comparison among various parameter extraction algorithms for single diode model of Photowatt-PWP201 module

Algorithms	I_{ph} (A)	I_0 (μA)	n_m	R_{sm} (Ω)	R_{shm} (Ω)	RMSE	NFEs
ISCE	1.0305143	3.48226304	48.642835	1.201271	981.98228038	**2.425075E−03**	**5000**
EHA-NMS [25]	1.0305143	3.48226292	48.642835	1.201271	981.98222618	**2.425075E−03**	**5000**
R_{cr}-IJADE [35]	1.0305143	3.48226290	48.642835	1.201271	981.98216000	2.425075E−03	10000
FPA [49]	1.032091	3.047538	48.13128	1.217583	811.3721	2.7425E−03	25000
MPCOA [39]	1.03188	3.37370	48.50646	1.20295	849.6927	2.4251E−03	250000
ABC-DE [31]	1.0318	3.2774	48.3948	1.2062	845.2495	3.8855E−03	120000

5.1.2. Accuracy for double diode model

For the double diode model of R.T.C. France solar cell at 33 °C [21], the parameter values and $RMSE_{cal}$ value extracted by proposed ISCE algorithm are summarized in Table 4, where the reported results of some recent algorithms are preferentially considered for comparison because of their good performance and available maximum number of function evaluations. It is evident from Table 4 that the proposed ISCE algorithm and EHA-NMS algorithm take the least number of function evaluations to get the most accurate $RMSE_{cal}$ value among all compared algorithms. This implies these two algorithms also have the highest computational efficiency in extracting the most accurate parameter values of double diode model.

To validate the accuracy of optimal parameter values extracted by ISCE algorithm, they are returned to Eq. (2) and *fezro* function is employed to reconstruct the simulated data of double diode model of R.T.C. France solar cell. The simulated and measured data are compared in Table 5 and Fig. 6 to observe the accordance between them.

It is clear from Fig. 6(a) and (c) that the simulated data of double diode model are in excellent accordance with the measured data almost in all data points. By cross checking Tables 3 and 5, Figs. 5 and 6, one can see from the simulated current data that the $RMSE_{sim}$ and the sum of IAE_{sim} of double diode model are smaller than those of single diode model, which further demonstrates the optimal parameter values extracted by ISCE algorithm are quite accurate. However, for the simulated power data, there is no guarantee that the $RMSE_{sim}$ and the sum of IAE_{sim} of double diode model are smaller than those of single diode model. The basic reason behind this is that the objective function in Eq. (5) is to minimize the errors between the calculated and measured

Table 7
Simulated results of ISCE algorithm for single diode model of Photowatt-PWP201 module.

Item	Measured data		Simulated current data		Simulated power data	
	V (V)	I (A)	I_{sim} (A)	IAE_{sim} (A)	P_{sim} (W)	IAE_{sim} (W)
1	0.1248	1.0315	1.02912209	0.00237791	0.12843444	0.00029676
2	1.8093	1.0300	1.02738435	0.00261565	1.85884651	0.00473249
3	3.3511	1.0260	1.02574214	0.00025786	3.43736448	0.00086412
4	4.7622	1.0220	1.02410399	0.00210399	4.87698803	0.01001963
5	6.0538	1.0180	1.02228341	0.00428341	6.18869931	0.02593091
6	7.2364	1.0155	1.01991740	0.00441740	7.38053027	0.03196607
7	8.3189	1.0140	1.01635081	0.00235081	8.45492077	0.01955617
8	9.3097	1.0100	1.01049143	0.00049143	9.40737206	0.00457506
9	10.2163	1.0035	1.00067876	0.00282124	10.22323441	0.02882264
10	11.0449	0.9880	0.98465335	0.00334665	10.87539777	0.03696343
11	11.8018	0.9630	0.95969741	0.00330259	11.32615687	0.03897653
12	12.4929	0.9255	0.92304875	0.00245125	11.53155579	0.03062316
13	13.1231	0.8725	0.87258816	0.00008816	11.45106168	0.00115693
14	13.6983	0.8075	0.80731012	0.00018988	11.05877623	0.00260102
15	14.2221	0.7265	0.72795782	0.00145782	10.35308888	0.02073323
16	14.6995	0.6345	0.63646618	0.00196618	9.35573459	0.02890184
17	15.1346	0.5345	0.53569607	0.00119607	8.10754576	0.01810206
18	15.5311	0.4275	0.42881615	0.00131615	6.65998648	0.02044123
19	15.8929	0.3185	0.31866866	0.00016866	5.06456910	0.00268045
20	16.2229	0.2085	0.20785711	0.00064289	3.37204517	0.01042948
21	16.5241	0.1010	0.09835421	0.00264579	1.62521481	0.04371929
22	16.7987	−0.0080	−0.00816934	0.00016934	−0.13723426	0.00284466
23	17.0499	−0.1110	−0.11096846	0.00003154	−1.89200116	0.00053774
24	17.2793	−0.2090	−0.20911762	0.00011762	−3.61340604	0.00203234
25	17.4885	−0.3030	−0.30202238	0.00097762	−5.28191833	0.01709717
Sum of IAE_{sim}				0.04178790		0.40460442
$RMSE_{sim}$				2.13852593E−03		2.11907567E−02

current data rather than the calculated and measured power data. Hence, objective function should be selected according to the specific application.

5.1.3. Accuracy for solar module model

For the single diode model of Photowatt-PWP201 module at 45 °C [21], the parameter extraction results of proposed ISCE algorithm are shown in Table 6 and compared with those of some recent algorithms, including EHA-NMS, R_{cr}-IJADE, FPA, MPCOA and ABC-DE. Similar to previous cases, ISCE algorithm and EHA-NMS algorithm still provide the optimal $RMSE_{cal}$ value with the least number of function evaluations among all compared algorithms.

Just like before, the optimal parameter values extracted by ISCE algorithm are substituted into Eq. (4) and *fezro* function is utilized to rebuild the simulated *I–V* data and *P–V* data. The simulated results are tabulated in Table 7 and plotted in Fig. 7 to contrast with the measured data. It is clear from Fig. 7(a) and (c) that the simulated data match the measured data nicely. The IAE_{sim} in Fig. 7(b) and (d) and their sum in Table 7 are very tiny comparing with the measured current data and power data. These put into evidence that the optimal parameter values extracted by ISCE algorithm achieve satisfying accuracy.

For the simulated *I–V* data, it must be pointed out that due to the inherently implicit nature of SDM Eq. (1), DDM Eq. (2) and SMM Eq. (4), whose $RMSE_{cal}$ value in Tables 2, 4 and 6 are always larger than their $RMSE_{sim}$ value in Tables 3, 5 and 7, respectively. Hence, the $RMSE_{sim}$ value, rather than the $RMSE_{cal}$ value, should be considered as the ultimate criterion for quantifying the accuracy of extracted parameters. Any reduction of $RMSE_{sim}$ value is of vital significance, because it results in improvement in the knowledge about the real values of the model parameters.

5.1.4. Convergence and robustness

The superior accuracy and computational efficiency of proposed ISCE algorithm has been confirmed by the comparison results in previous subsections. Yet it would be premature to conclude that the proposed ISCE algorithm surpasses other algorithms in this area, mainly because the parameter extraction results shown above may be the best one. Hence, it is very necessary to further investigate its convergence and robustness through the statistical results of a large number of independent runs. According to the comparison results in previous subsections, EHA-NMS [25] and R_{cr}-IJADE [35] algorithms are most competitive to our proposed ISCE algorithm. Hence, the convergence and robustness of these three algorithms are directly compared in this subsection.

Under the same searching ranges, the average convergence curve of 1000 independent runs of ISCE, EHA-NMS and R_{cr}-IJADE algorithms are illustrated in Figs. 8–10(a), indicating different average $RMSE_{cal}$ values during the parameter extraction process of SDM, DDM and SMM, respectively. It is evident that the proposed ISCE algorithm converges much faster than EHA-NMS and R_{cr}-IJADE algorithms, because most of its average convergence curves are lower than EHA-NMS and R_{cr}-IJADE algorithms, as evidenced by the DataTips in Figs. 8–10(a). For the single diode model in Figs. 8 and 10(a), the final average $RMSE_{cal}$ values of ISCE and EHA-NMS algorithms are identical with those of R_{cr}-IJADE algorithm, despite the number of function evaluations of ISCE and EHA-NMS algorithms are only half that of R_{cr}-IJADE algorithm. This further confirms the superior computational efficiency of proposed ISCE algorithm. For the double diode model in Fig. 9(a), the final average $RMSE_{cal}$ value of ISCE algorithm is smaller than that of R_{cr}-IJADE algorithm but larger than that of EHA-NMS algorithm, which proves the convergence performance of ISCE algorithm lies between R_{cr}-IJADE and EHA-NMS algorithms. Moreover, one can see from Fig. 9(a) that there is a turning point at $NFEs = 2000$ on the average convergence curve of ISCE algorithm, which corresponds to the end of additional constraint presented in Section 4.2.2. It is clear from Fig. 9(a) that before the turning point, ISCE algorithm converges very slowly, which suggests the additional constraint is very much a double-edged sword, reducing the probability of DDM Eq. (2) degenerates into SDM Eq. (1) while decreasing the convergence speed of ISCE algorithm.

The statistical results of 1000 independent runs of ISCE, EHA-NMS and R_{cr}-IJADE algorithms are summarized in Table 8, where NFEs@thV records the number of function evaluations at which the $RMSE_{cal}$ value

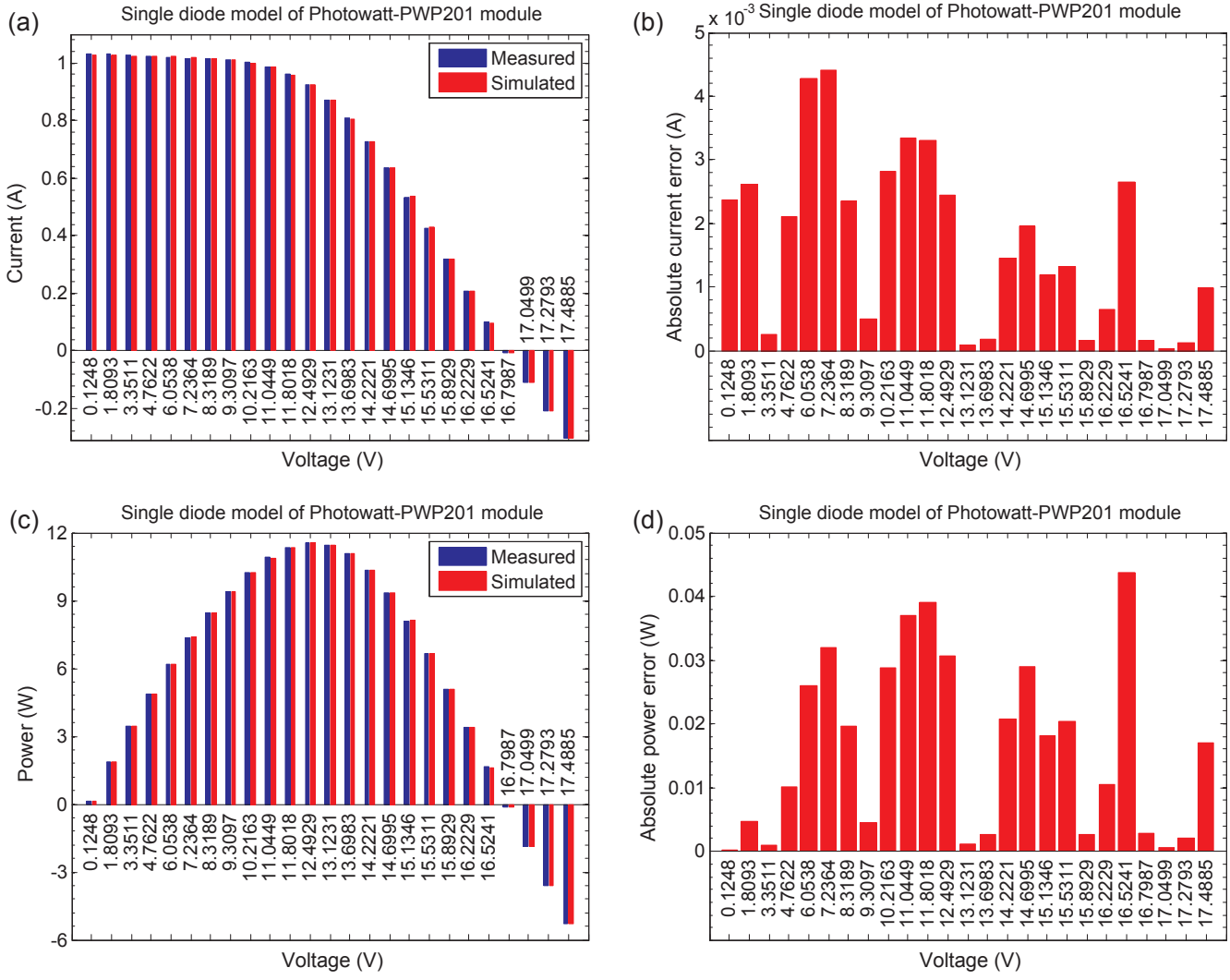

Fig. 7. Comparison between the measured data and the simulated data obtained by ISCE algorithm for single diode model of Photowatt-PWP201 module: (a) *I–V* data, (b) Absolute current error, (c) *P–V* data and (d) Absolute power error.

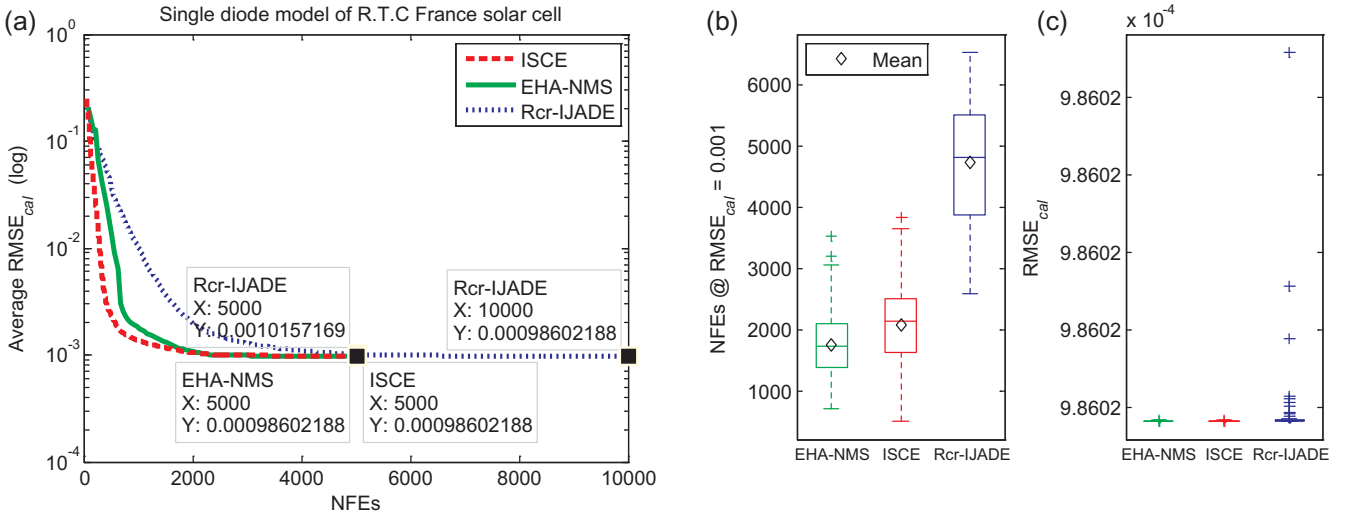

Fig. 8. Statistical graphs of 1000 independent runs of ISCE, EHA-NMS and R_{cr}-IJADE algorithms for parameter extraction of single diode model. (a) Average convergence curves, (b) Box plots of the NFEs at $RMSE_{cal} = 0.001$ and (c) Box plots of $RMSE_{cal}$ value of each run.

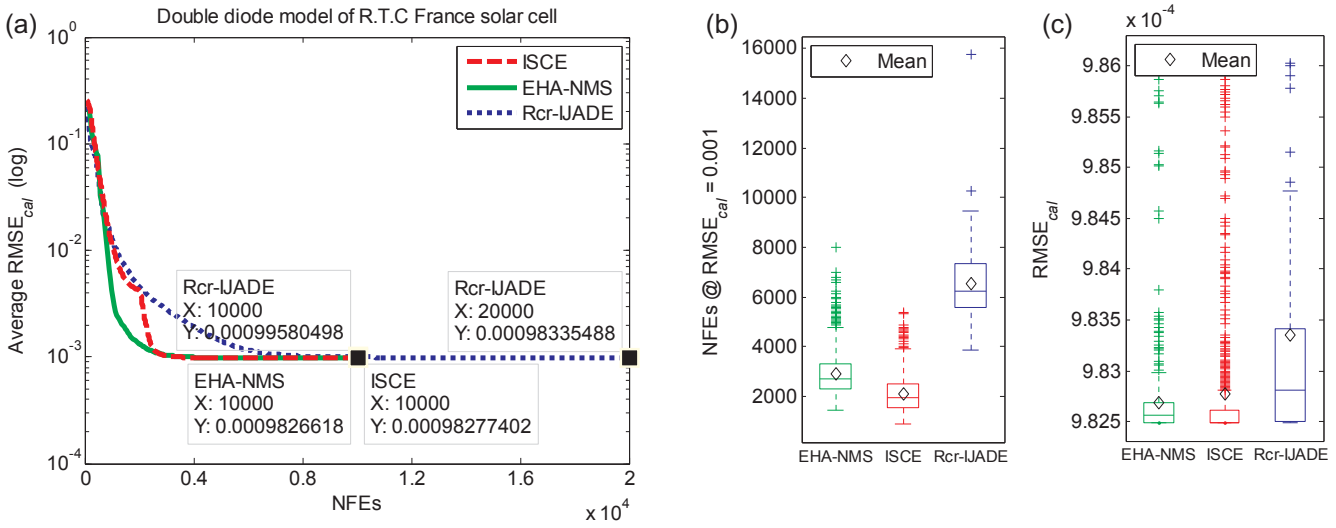

Fig. 9. Statistical graphs of 1000 independent runs of ISCE, EHA-NMS and R_{cr}-IJADE algorithms for parameter extraction of double diode model. (a) Average convergence curves, (b) Box plots of the NFEs at $RMSE_{cal} = 0.001$ and (c) Box plots of $RMSE_{cal}$ value of each run.

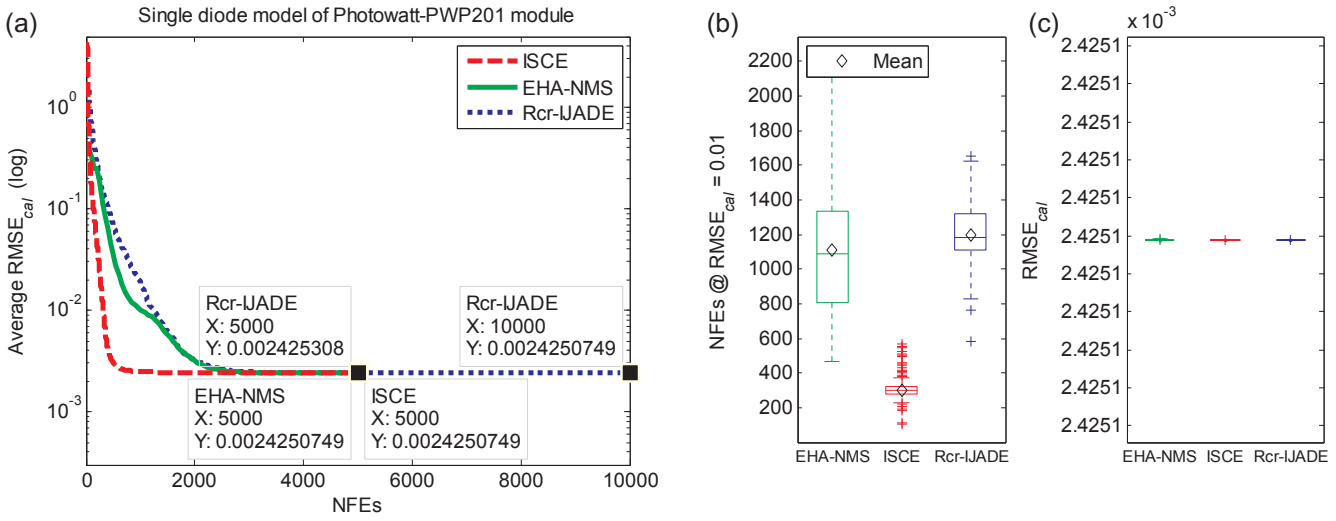

Fig. 10. Statistical graphs of 1000 independent runs of ISCE, EHA-NMS and R_{cr}-IJADE algorithms for parameter extraction of solar module model. (a) Average convergence curves, (b) Box plots of the NFEs at $RMSE_{cal} = 0.01$ and (c) Box plots of $RMSE_{cal}$ value of each run.

Table 8
Statistical results of 1000 independent runs of ISCE, EHA-NMS and R_{cr}-IJADE algorithms for parameter extraction of different PV models. NFEs@thV records the number of function evaluations at which the $RMSE_{cal}$ value is equal or less than threshold value (thV), hereinafter.

Solar cell/modules and thV	Models	Algorithms	NFEs@thV		$RMSE_{cal}$			
			Mean	Std	Min	Mean	Max	Std
R.T.C. France solar cell thV = 0.001	SDM	ISCE	2072	644	9.860219E−04	9.860219E−04	9.860219E−04	3.98E−17
		EHA-NMS	1755	475	9.860219E-04	9.860219E-04	9.860219E-04	6.64E−17
		R_{cr}-IJADE	4735	948	9.860219E−04	9.860219E−04	9.860219E−04	3.10E−14
R.T.C. France solar cell thV = 0.001	DDM	ISCE	2122	757	9.824849E-04	9.827740E−04	9.861092E-04	4.61E−07
		EHA-NMS	2908	848	9.824849E-04	9.826829E−04	9.860219E-04	5.19E−07
		R_{cr}-IJADE	6523	1551	9.824849E−04	9.833549E−04	9.860234E−04	1.20E−06
Photowatt-PWP201 module thV = 0.01	SMM	ISCE	303	41	2.425075E−03	2.425075E−03	2.425075E−03	2.47E−17
		EHA-NMS	1113	344	2.425075E-03	2.425075E-03	2.425075E-03	5.53E−17
		R_{cr}-IJADE	1200	204	2.425075E−03	2.425075E−03	2.425075E−03	2.51E−17

is equal or less than the threshold value (**thV**). It is clear from Table 8 that all the mean NFEs@thV of ISCE and EHA-NMS algorithms are remarkably smaller than that of R_{cr}-IJADE algorithm, as evidenced by Figs. 8–10(b). For the first case, the mean NFEs@thV of ISCE algorithm is little bigger than that of EHA-NMS algorithm. However, in the other two cases, the mean NFEs@thV of ISCE algorithm is much smaller than that of EHA-NMS algorithm. These results prove that ISCE algorithm generally converges better than EHA-NMS and R_{cr}-IJADE algorithms.

The distributions of final $RMSE_{cal}$ value for each independent run of ISCE, EHA-NMS and R_{cr}-IJADE algorithms are plotted in Figs. 8–10(c).

Table 9
Simulated results of ISCE algorithm for single diode model of STM6-40/36 module

Item	Measured data		Simulated current data		Simulated power data	
	V (V)	I (A)	I_{sim} (A)	IAE_{sim} (A)	P_{sim} (W)	IAE_{sim} (W)
1	0	1.663	1.66345813	0.00045813	0	0
2	0.118	1.663	1.66325224	0.00025224	0.19626376	0.00002976
3	2.237	1.661	1.65955120	0.00144880	3.71241603	0.00324097
4	5.434	1.653	1.65391444	0.00091444	8.98737109	0.00496909
5	7.260	1.650	1.65056575	0.00056575	11.98310732	0.00410732
6	9.680	1.645	1.64543044	0.00043044	15.92776663	0.00416663
7	11.59	1.640	1.63923405	0.00076595	18.99872263	0.00887737
8	12.60	1.636	1.63371510	0.00228490	20.58481021	0.02878979
9	13.37	1.629	1.62728848	0.00171152	21.75684699	0.02288301
10	14.09	1.619	1.61831518	0.00068482	22.80206083	0.00964917
11	14.88	1.597	1.60306738	0.00606738	23.85364261	0.09028261
12	15.59	1.581	1.58158500	0.00058500	24.65691009	0.00912009
13	16.40	1.542	1.54232745	0.00032745	25.29417018	0.00537018
14	16.71	1.524	1.52122497	0.00277503	25.41966933	0.04637067
15	16.98	1.500	1.49920572	0.00079428	25.45651314	0.01348686
16	17.13	1.485	1.48527115	0.00027115	25.44269473	0.00464473
17	17.32	1.465	1.46564321	0.00064321	25.38494047	0.01114047
18	17.91	1.388	1.38759934	0.00040066	24.85190419	0.00717581
19	19.08	1.118	1.11837210	0.00037210	21.33853972	0.00709972
20	21.02	0	−0.00002131	0.00002131	−0.00044802	0.00044802
Sum of IAE_{sim}				0.02177457		0.281852285
$RMSE_{sim}$				1.72192793E−03		0.024936627

Table 10
Simulated results of ISCE algorithm for single diode model of STP6-120/36 module

Item	Measured data		Simulated current data		Simulated power data	
	V (V)	I (A)	I_{sim} (A)	IAE_{sim} (A)	P_{sim} (W)	IAE_{sim} (W)
1	0	7.48	7.47098129	0.00901871	0	0
2	9.06	7.45	7.45253755	0.00253755	67.51999023	0.02299023
3	9.74	7.42	7.44671497	0.02671497	72.53100378	0.26020378
4	10.32	7.44	7.43909223	0.00090777	76.77143185	0.00936815
5	11.17	7.41	7.42026500	0.01026500	82.88436007	0.11466007
6	11.81	7.38	7.39587314	0.01587314	87.34526184	0.18746184
7	12.36	7.37	7.36326479	0.00673521	91.00995283	0.08324717
8	12.74	7.34	7.33148307	0.00851693	93.40309430	0.10850570
9	13.16	7.29	7.28412985	0.00587015	95.85914884	0.07725116
10	13.59	7.23	7.21776060	0.01223940	98.08936657	0.16633343
11	14.17	7.10	7.08813731	0.01186269	100.43890574	0.16809426
12	14.58	6.97	6.95844905	0.01155095	101.45418713	0.16841287
13	14.93	6.83	6.81486011	0.01513989	101.74586140	0.22603860
14	15.39	6.58	6.56792937	0.01207063	101.08043295	0.18576705
15	15.71	6.36	6.34872742	0.01127258	99.73850783	0.17709217
16	16.08	6.00	6.03749239	0.03749239	97.08287760	0.60287760
17	16.34	5.75	5.77681380	0.02681380	94.39313753	0.43813753
18	16.76	5.27	5.27376516	0.00376516	88.38830402	0.06310402
19	16.9	5.07	5.08193389	0.01193389	85.88468270	0.20168270
20	17.1	4.79	4.78583302	0.00416698	81.83774456	0.07125544
21	17.25	4.56	4.54628941	0.01371059	78.42349234	0.236507657
22	17.41	4.29	4.27392907	0.01607093	74.40910507	0.27979493
23	17.65	3.83	3.83228232	0.00228232	67.63978288	0.04028288
24	19.21	0	0.00116434	0.00116434	0.02236705	0.02236705
Sum of IAE_{sim}				0.27797597		3.91143627
$RMSE_{sim}$				1.44183790E−02		0.21252820

Table 11
Comparison among various parameter extraction algorithms for single diode model of STM6-40/36 module

Algorithms	I_{ph} (A)	I_0 (μA)	n	R_s (mΩ)	R_{sh} (Ω)	RMSE	NFEs
ISCE	1.66390478	1.73865691	1.52030292	4.27377125	15.92829413	**1.72981371E−03**	**5000**
EHA-NMS [25]	1.66390478	1.73865691	1.52030292	4.27377125	15.92829417	**1.72981371E−03**	**5000**
R_{cr}-IJADE [35]	1.66390480	1.73865690	1.52030292	4.27377139	15.92829417	1.72981371E−03	10000
TMP [73]	1.6635	1.4142	1.4986	4.879	15.419	3.11854870E−03	NA

Table 12
Comparison among various parameter extraction algorithms for single diode model of STP6-120/36 module

Algorithms	I_{ph} (A)	I_0 (μA)	n	R_s (mΩ)	R_{sh} (Ω)	RMSE	NFEs
ISCE	7.47252992	2.33499500	1.26010348	4.59463460	22.21990556	**1.66006031E−02**	**5000**
EHA-NMS [25]	7.47252992	2.33499510	1.26010348	4.59463459	22.21990350	**1.66006031E−02**	**5000**
R_{cr}-IJADE [35]	7.47252990	2.33499470	1.26010347	4.59463472	22.21989750	1.66006031E−02	10000
TMP [73]	7.4838	1.2	1.2072	4.9	9.745	2.37103855E−02	NA

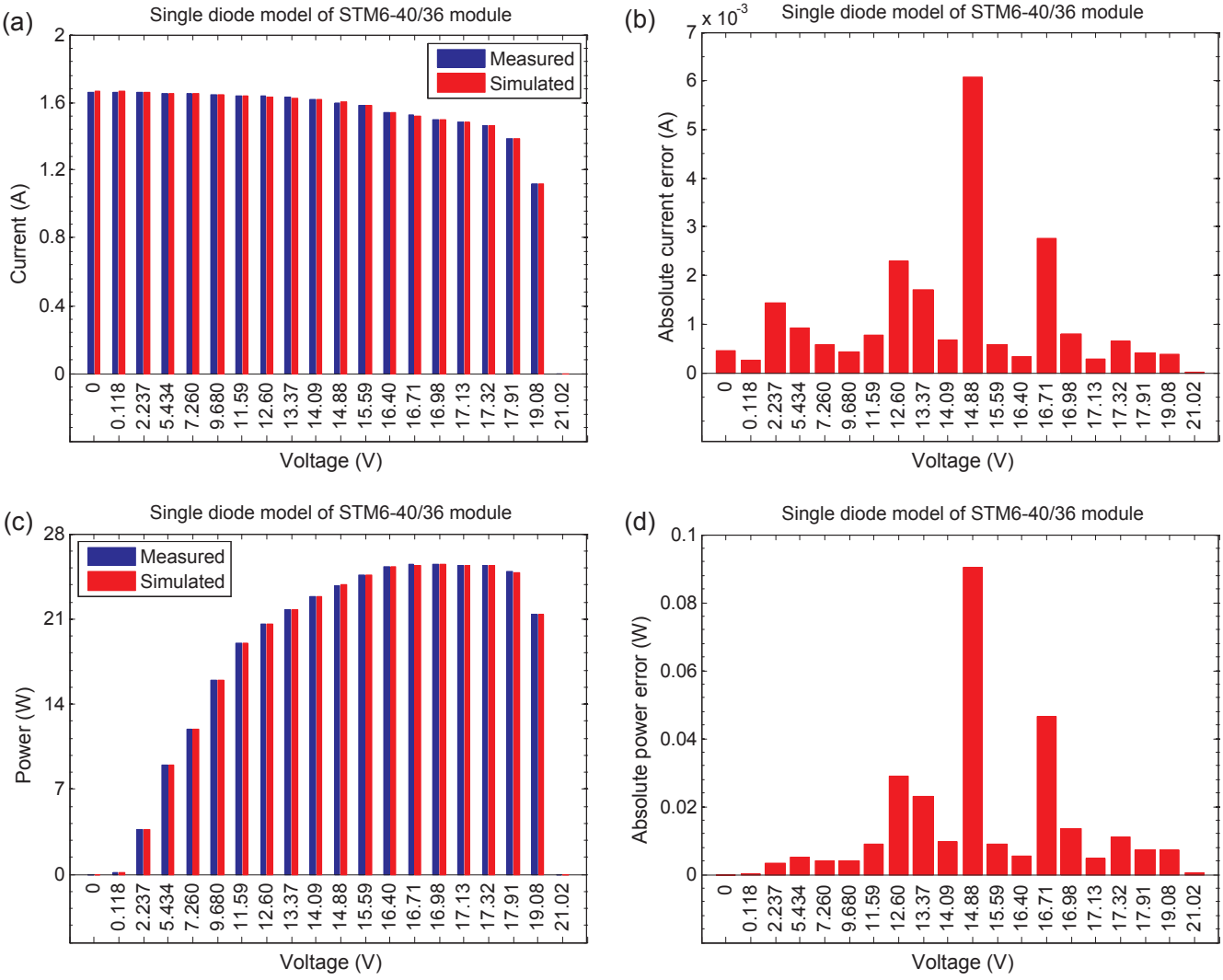

Fig. 11. Comparison between the measured data and the simulated data obtained by ISCE algorithm for single diode model of STM6-40/36 module: (a) *I–V* data, (b) Absolute current error, (c) *P–V* data and (d) Absolute power error.

One can see from Figs. 8–10(c) and Table 8 that the mean $RMSE_{cal}$ values of the three algorithms can be generally sorted as: EHA-NMS ≤ ISCE ≤ R_{cr}-IJADE. This indicates that ISCE algorithm is super to R_{cr}-IJADE algorithm but lightly infer to EHA-NMS algorithm in terms of average accuracy. It is clear from Fig. 9(c) that the box of ISCE algorithm is much smaller than that of EHA-NMS and R_{cr}-IJADE algorithms, while there is no obvious difference between the boxes in Figs. 8 and 10(c). In Table 8, according to the standard deviation of $RMSE_{cal}$ value, the three algorithms can be generally sorted as: ISCE < EHA-NMS < R_{cr}-IJADE. This reveals that ISCE algorithm is superior R_{cr}-IJADE and EHA-NMS algorithms in terms of robustness.

5.2. Results on practical measured datasets

In addition to the standard datasets, the practical measured *I–V* data of a mono-crystalline STM6-40/36 module at 51 °C and a polycrystalline STP6-120/36 module at 55 °C [73] are considered for investigating the applicability of proposed ISCE algorithm. As shown in Tables 9 and 10, these two sets of practical measured *I–V* data are very typical, because the former lacks the measurements near open-circuit voltage while the latter lacks the measurements near both short-circuit current and open-circuit voltage.

The optimal parameter values and $RMSE_{cal}$ value extracted by proposed ISCE algorithm for these two sets of practical measured *I–V* data are reported in Tables 11 and 12, respectively. For comparison, the parameter extraction results of EHA-NMS [25], R_{cr}-IJADE [35] and TMP [73] algorithms are also listed there. It is obvious that the proposed ISCE and EHA-NMS algorithms still require the least number of function evaluations to acquire the optimal $RMSE_{cal}$ value. This suggests that the proposed ISCE algorithm consistently provides superior

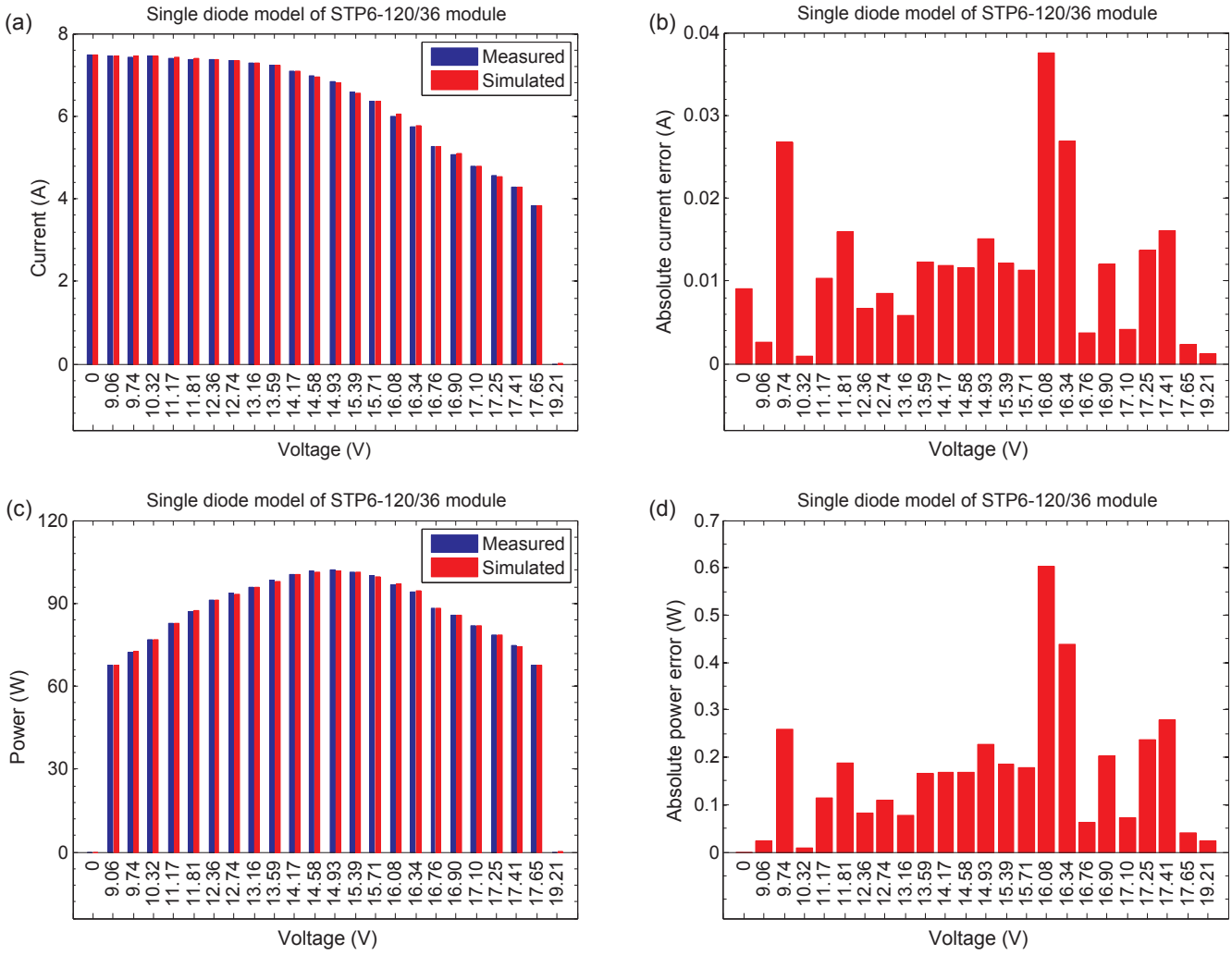

Fig. 12. Comparison between the measured data and the simulated data obtained by ISCE algorithm for single diode model of STP6-120/36 module: (a) *I–V* data, (b) Absolute current error, (c) *P–V* data and (d) Absolute power error.

Table 13
Statistical results of 1000 independent runs of ISCE, EHA-NMS and R_{cr}-IJADE algorithms for parameter extraction of STM6-40/36 module and STP6-120/36 module.

Solar modules and thV	Algorithms	NFEs@thV		$RMSE_{cal}$			
		Mean	Std	Min	Mean	Max	Std
STM6-40/36 module	ISCE	1122	449	1.729814E−03	1.729814E−03	1.729814E−03	2.30E−17
thV = 0.002	EHA-NMS	1645	311	1.729814E−03	1.729814E−03	1.729814E−03	2.43E−17
	R_{cr}-IJADE	2972	606	1.729814E−03	1.729814E−03	1.729814E−03	1.18E−14
STP6-120/36 module	ISCE	788	246	1.660060E−02	1.660060E−02	1.660060E−02	8.74E−14
thV = 0.02	EHA-NMS	1216	231	1.660060E−02	1.660064E−02	1.664184E−02	1.30E−06
	R_{cr}-IJADE	2562	490	1.660060E−02	1.660060E−02	1.660060E−02	1.29E−14

computational efficiency and the most accurate parameter values of solar modules.

The simulated results reconstructed by the optimal parameter values of ISCE algorithm are listed in Tables 9 and 10, respectively. For easy comparison and crosschecking, they are respectively illustrated in Figs. 11 and 12 to compare with the measured data. It is clear that there is only tiny difference between the simulated data and measured data. The IAE_{sim} in Figs. 11 and 12, their sum in Tables 9 and 10 are inappreciable in comparison with the measured data. Therefore, the accuracy of ISCE algorithm is manifested to be universal and reliable.

The statistical results of 1000 independent runs of ISCE, EHA-NMS and R_{cr}-IJADE algorithms are summarized in Table 13, Figs. 13 and 14, respectively. One can see from Figs. 13–14(a) that proposed ISCE algorithm still converges much faster than EHA-NMS and R_{cr}-IJADE algorithms, because all its average convergence curves are lower than EHA-NMS and R_{cr}-IJADE algorithms. From Table 13, it is evident that the mean NFEs@thV of ISCE algorithm is significantly smaller than that of EHA-NMS and R_{cr}-IJADE algorithms, as evidenced by Figs. 13–14(b). One can see from Figs. 13–14(c) and Table 13 that ISCE algorithm is more robust than EHA-NMS and R_{cr}-IJADE algorithms in terms of the standard deviation of $RMSE_{cal}$ value. All above results conclude that, comparing with EHA-NMS and R_{cr}-IJADE algorithms, ISCE algorithm has superior convergence and robustness under the same accuracy for the single diode model of practical measured *I–V* data of solar modules.

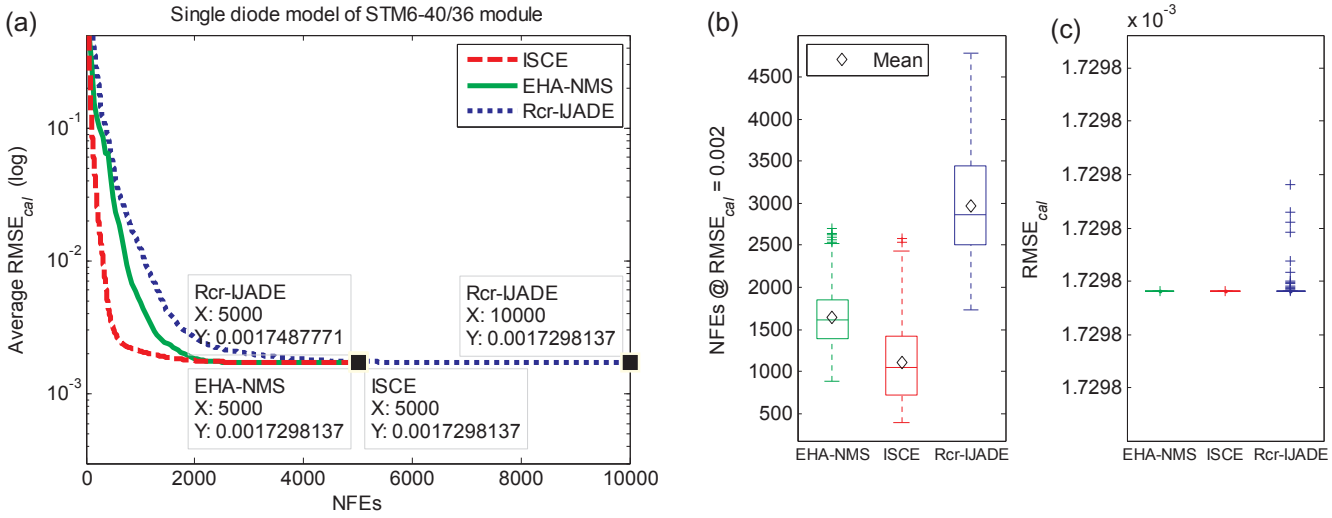

Fig. 13. Statistical graphs of 1000 independent runs of ISCE, EHA-NMS and R_{cr}-IJADE algorithms for parameter extraction of STP6-120/36 module. (a) Average convergence curves, (b) Box plots of the NFEs at $RMSE_{cal}$ = 0.002 and (c) Box plots of $RMSE_{cal}$ value of each run.

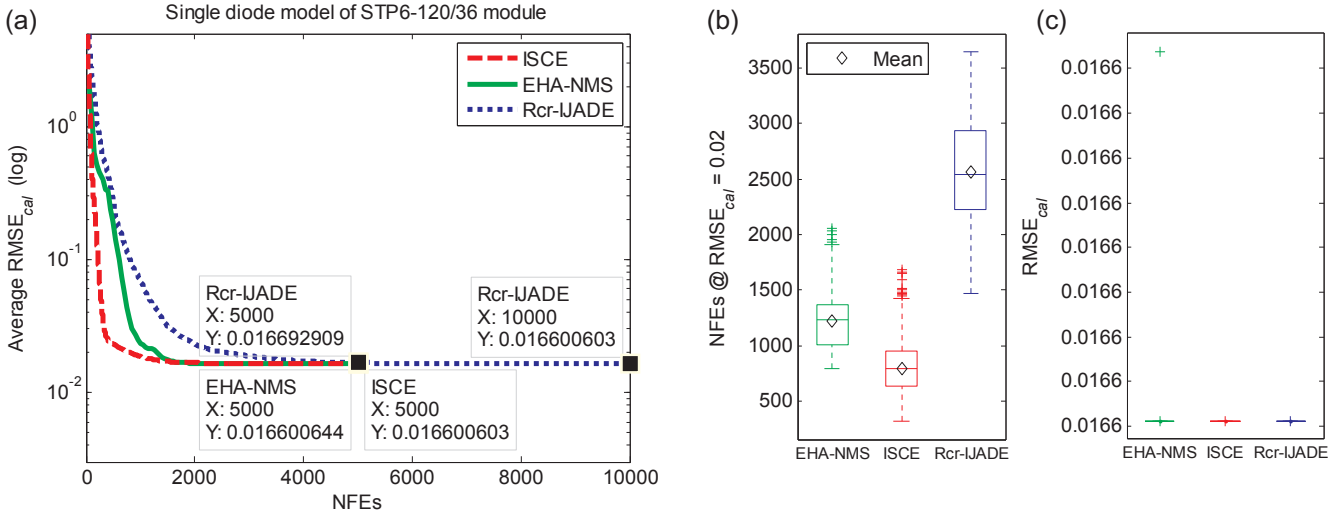

Fig. 14. Statistical graphs of 1000 independent runs of ISCE, EHA-NMS and R_{cr}-IJADE algorithms for parameter extraction of STM6-40/36 module. (a) Average convergence curves, (b) Box plots of the NFEs at $RMSE_{cal}$ = 0.02 and (c) Box plots of $RMSE_{cal}$ value of each run.

6. Conclusion

In this paper, an improved shuffled complex evolution algorithm is proposed for fast and accurately parameter extraction of different solar cell models. The innovation of proposed ISCE algorithm lies primary in the improved CCE strategy, where three amendments are proposed to enhance the evolution efficiency of original CCE strategy. Firstly, the expansion step and outside contraction step are inserted to improve the probability of producing better qualified offspring. Secondly, in order to enhance the chance of global search and avoid being trapped in local minima, the reflecting-absorbing bound-handling method is adopted to replace the random mutation within the smallest hypercube. Ultimately, in order to overcome the local roughness and drive the simplex evolution in an efficient manner, the main diagonal of simplex is adopted to replace the worst vertex when inside contraction step failed to produce qualified offspring. The combination of these amendments can largely ensure the population evolving continuously toward the global optimum.

The performance of proposed ISCE algorithm is comprehensively evaluated through the parameter extraction problems of SDM, DDM and SMM of various solar cell/modules. Additionally, an intensive performance comparison with some state-of-the-art algorithms is made to further demonstrate the superiority of proposed ISCE algorithm. Comparison results from both standard datasets and practical measured datasets indicate that the proposed ISCE algorithm always exhibits the highest computational efficiency to get the most accurate parameter values among all compared algorithms. Compared to the reported state-of-the-art algorithms, the proposed ISCE algorithm usually promises better convergence and robustness. Therefore, the proposed ISCE algorithm is an accurate, efficient and reliable approach for solving the parameter extraction problem of solar cell models.

Acknowledgments

The authors would like to thank the anonymous reviewers for their constructive suggestions. The authors gratefully acknowledge Dr. Wenyin Gong and Dr. Zhicong Chen for their generous offer of the source codes of R_{cr}-IJADE and EHA-NMS algorithms. This work was supported by the Plan For Scientific Innovation Talent of Henan Province [Grant Number 174100510020], Henan province institution of higher learning youth backbone teachers training program [Grant Number 2016GGJS-0360], the Program for Science & Technology

Innovation Talents in Universities of Henan Province [grant number 16HASTIT026] and the National Natural Science Foundation of China [Grant Numbers 51576060 and U1304528].

References

[1] Femia N, Petrone G, Spagnuolo G, Vitelli M. Power electronics and control techniques for maximum energy harvesting in photovoltaic systems. CRC Press; 2012.

[2] Batzelis EI, Kampitsis GE, Papathanassiou SA, Manias SN. Direct MPP calculation in terms of the single-diode PV model parameters. IEEE Trans Energy Convers 2015;30:226–36. http://dx.doi.org/10.1109/TEC.2014.2356017.

[3] Chin VJ, Salam Z, Ishaque K. Cell modelling and model parameters estimation techniques for photovoltaic simulator application: a review. Appl Energy 2015;154:500–19. http://dx.doi.org/10.1016/j.apenergy.2015.05.035.

[4] Jordehi AR. Parameter estimation of solar photovoltaic (PV) cells: a review. Renew Sustain Energy Rev 2016;61:354–71. http://dx.doi.org/10.1016/j.rser.2016.03.049.

[5] Humada AM, Hojabri M, Mekhilef S, Hamada HM. Solar cell parameters extraction based on single and double-diode models: a review. Renew Sustain Energy Rev 2016;56:494–509. http://dx.doi.org/10.1016/j.rser.2015.11.051.

[6] Muhsen DH, Ghazali AB, Khatib T, Abed IA. Parameters extraction of double diode photovoltaic module's model based on hybrid evolutionary algorithm. Energy Convers Manage 2015;105:552–61. http://dx.doi.org/10.1016/j.enconman.2015.08.023.

[7] Chin VJ, Salam Z, Ishaque K. An accurate modelling of the two-diode model of PV module using a hybrid solution based on differential evolution. Energy Convers Manage 2016;124:42–50. http://dx.doi.org/10.1016/j.enconman.2016.06.076.

[8] Awadallah MA. Variations of the bacterial foraging algorithm for the extraction of PV module parameters from nameplate data. Energy Convers Manage 2016;113:312–20. http://dx.doi.org/10.1016/j.enconman.2016.01.071.

[9] Barth N, Jovanovic R, Ahzi S, Khaleel MA. PV panel single and double diode models: optimization of the parameters and temperature dependence. Sol Energy Mater Sol Cells 2016;148:87–98. http://dx.doi.org/10.1016/j.solmat.2015.09.003.

[10] Dileep G, Singh SN. Application of soft computing techniques for maximum power point tracking of SPV system. Sol Energy 2017;141:182–202. http://dx.doi.org/10.1016/j.solener.2016.11.034.

[11] R. Benkercha, S. Moulahoum, I. Colak, B. Taghezouit. PV module parameters extraction with maximum power point estimation based on flower pollination algorithm. In: 2016 IEEE International Power Electronics and Motion Control Conference (PEMC); 2016. p. 442–9. doi: http://dx.doi.org/10.1109/EPEPEMC.2016.7752038.

[12] Koohi-Kamali S, Rahim NA, Mokhlis H, Tyagi VV. Photovoltaic electricity generator dynamic modeling methods for smart grid applications: a review. Renew Sustain Energy Rev 2016;57:131–72. http://dx.doi.org/10.1016/j.rser.2015.12.137.

[13] Kharb RK, Shimi SL, Chatterji S, Ansari MF. Modeling of solar PV module and maximum power point tracking using ANFIS. Renew Sustain Energy Rev 2014;33:602–12. http://dx.doi.org/10.1016/j.rser.2014.02.014.

[14] Liu Y, Li M, Ji X, Luo X, Wang M, Zhang Y. A comparative study of the maximum power point tracking methods for PV systems. Energy Convers Manage 2014;85:809–16. http://dx.doi.org/10.1016/j.enconman.2014.01.049.

[15] Fathabadi H. Two novel techniques for increasing energy efficiency of photovoltaic-battery systems. Energy Convers Manage 2015;105:149–66. http://dx.doi.org/10.1016/j.enconman.2015.07.036.

[16] Kheldoun A, Bradai R, Boukenoui R, Mellit A. A new Golden Section method-based maximum power point tracking algorithm for photovoltaic systems. Energy Convers Manage 2016;111:125–36. http://dx.doi.org/10.1016/j.enconman.2015.12.039.

[17] Gao X, Cui Y, Hu J, Xu G, Yu Y. Lambert W-function based exact representation for double diode model of solar cells: comparison on fitness and parameter extraction. Energy Convers Manage 2016;127:443–60. http://dx.doi.org/10.1016/j.enconman.2016.09.005.

[18] Ortiz-Conde A, García Sánchez FJ, Muci J. New method to extract the model parameters of solar cells from the explicit analytic solutions of their illuminated I-V characteristics. Sol Energy Mater Sol Cells 2006;90:352–61. http://dx.doi.org/10.1016/j.solmat.2005.04.023.

[19] Zhang C, Zhang J, Hao Y, Lin Z, Zhu C. A simple and efficient solar cell parameter extraction method from a single current-voltage curve. J Appl Phys 2011;110:064504–64507. http://dx.doi.org/10.1063/1.3632971.

[20] Ishaque K, Salam Z, Taheri H, Shamsudin A. A critical evaluation of EA computational methods for Photovoltaic cell parameter extraction based on two diode model. Sol Energy 2011;85:1768–79. http://dx.doi.org/10.1016/j.solener.2011.04.015.

[21] Easwarakhanthan T, Bottin J, Bouhouch I, Boutrit C. Nonlinear minimization algorithm for determining the solar cell parameters with microcomputers. Int J Solar Energy 1986;4:1–12. http://dx.doi.org/10.1080/01425918608909835.

[22] El-Naggar KM, AlRashidi MR, AlHajri MF, Al-Othman AK. Simulated annealing algorithm for photovoltaic parameters identification. Sol Energy 2012;86:266–74. http://dx.doi.org/10.1016/j.solener.2011.09.032.

[23] Dkhichi F, Oukarfi B, Fakkar A, Belbounaguia N. Parameter identification of solar cell model using Levenberg–Marquardt algorithm combined with simulated annealing. Sol Energy 2014;110:781–8. http://dx.doi.org/10.1016/j.solener.2014.09.033.

[24] AlHajri MF, El-Naggar KM, AlRashidi MR, Al-Othman AK. Optimal extraction of solar cell parameters using pattern search. Renewable Energy 2012;44:238–45. http://dx.doi.org/10.1016/j.renene.2012.01.082.

[25] Chen Z, Wu L, Lin P, Wu Y, Cheng S. Parameters identification of photovoltaic models using hybrid adaptive Nelder-Mead simplex algorithm based on eagle strategy. Appl Energy 2016;182:47–57. http://dx.doi.org/10.1016/j.apenergy.2016.08.083.

[26] Hamid NFA, Rahim NA, Selvaraj J. Solar cell parameters identification using hybrid Nelder-Mead and modified particle swarm optimization. J Renewable Sustainable Energy 2016;8. http://dx.doi.org/10.1063/1.4941791.

[27] Gao X, Yao C, Gao X, Yu Y. Accuracy comparison between implicit and explicit single-diode models of photovoltaic cells and modules. Acta Phys Sin 2014;63:178401. http://dx.doi.org/10.7498/aps.63.178401.

[28] AlRashidi MR, AlHajri MF, El-Naggar KM, Al-Othman AK. A new estimation approach for determining the I-V characteristics of solar cells. Sol Energy 2011;85:1543–50. http://dx.doi.org/10.1016/j.solener.2011.04.013.

[29] W. Huang, C. Jiang, L. Xue, D. Song. Extracting solar cell model parameters based on chaos particle swarm algorithm. In: 2011 International conference on electric information and control engineering; 2011. p. 398–402. doi: http://dx.doi.org/10.1109/ICEICE.2011.5777246.

[30] Meiying Y, Xiaodong W, Yousheng X. Parameter extraction of solar cells using particle swarm optimization. J Appl Phys 2009;105:094502–94508. http://dx.doi.org/10.1063/1.3122082.

[31] Hachana O, Hemsas KE, Tina GM, Ventura C. Comparison of different metaheuristic algorithms for parameter identification of photovoltaic cell/module. J Renewable Sustainable Energy 2013;5:053122. http://dx.doi.org/10.1063/1.4822054.

[32] Ma J, Man KL, Guan SU, Ting TO, Wong PWH. Parameter estimation of photovoltaic model via parallel particle swarm optimization algorithm. Int J Energy Res 2016;40:343–52. http://dx.doi.org/10.1002/er.3359.

[33] Jordehi AR. Time varying acceleration coefficients particle swarm optimisation (TVACPSO): a new optimisation algorithm for estimating parameters of PV cells and modules. Energy Convers Manage 2016;129:262–74. http://dx.doi.org/10.1016/j.enconman.2016.09.085.

[34] Jiang LL, Maskell DL, Patra JC. Parameter estimation of solar cells and modules using an improved adaptive differential evolution algorithm. Appl Energy 2013;112:185–93. http://dx.doi.org/10.1016/j.apenergy.2013.06.004.

[35] Gong W, Cai Z. Parameter extraction of solar cell models using repaired adaptive differential evolution. Sol Energy 2013;94:209–20. http://dx.doi.org/10.1016/j.solener.2013.05.007.

[36] Niu Q, Zhang L, Li K. A biogeography-based optimization algorithm with mutation strategies for model parameter estimation of solar and fuel cells. Energy Convers Manage 2014;86:1173–85. http://dx.doi.org/10.1016/j.enconman.2014.06.026.

[37] Chellaswamy C, Ramesh R. Parameter extraction of solar cell models based on adaptive differential evolution algorithm. Renewable Energy 2016;97:823–37. http://dx.doi.org/10.1016/j.renene.2016.06.024.

[38] Zhang Y, Lin P, Chen Z, Cheng S. A population classification evolution algorithm for the parameter extraction of solar cell models. Int J Photoenergy 2016;2016:1–16. http://dx.doi.org/10.1155/2016/2174573.

[39] Yuan X, Xiang Y, He Y. Parameter extraction of solar cell models using mutative-scale parallel chaos optimization algorithm. Sol Energy 2014;108:238–51. http://dx.doi.org/10.1016/j.solener.2014.07.013.

[40] Yuan X, He Y, Liu L. Parameter extraction of solar cell models using chaotic asexual reproduction optimization. Neural Comput Appl 2015;26:1227–39. http://dx.doi.org/10.1007/s00521-014-1795-6.

[41] Askarzadeh A, Rezazadeh A. Parameter identification for solar cell models using harmony search-based algorithms. Sol Energy 2012;86:3241–9. http://dx.doi.org/10.1016/j.solener.2012.08.018.

[42] Chen X, Yu K, Du W, Zhao W, Liu G. Parameters identification of solar cell models using generalized oppositional teaching learning based optimization. Energy 2016;99:170–80. http://dx.doi.org/10.1016/j.energy.2016.01.052.

[43] Niu Q, Zhang H, Li K. An improved TLBO with elite strategy for parameters identification of PEM fuel cell and solar cell models. Int J Hydrogen Energy 2014;39:3837–54. http://dx.doi.org/10.1016/j.ijhydene.2013.12.110.

[44] Patel SJ, Panchal AK, Kheraj V. Extraction of solar cell parameters from a single current–voltage characteristic using teaching learning based optimization algorithm. Appl Energy 2014;119:384–93. http://dx.doi.org/10.1016/j.apenergy.2014.01.027.

[45] Fathy A, Rezk H. Parameter estimation of photovoltaic system using imperialist competitive algorithm. Renewable Energy 2017;111:307–20. http://dx.doi.org/10.1016/j.renene.2017.04.014.

[46] Oliva D, Cuevas E, Pajares G. Parameter identification of solar cells using artificial bee colony optimization. Energy 2014;72:93–102. http://dx.doi.org/10.1016/j.energy.2014.05.011.

[47] Jamadi M, Merrikh-Bayat F, Bigdeli M. Very accurate parameter estimation of single- and double-diode solar cell models using a modified artificial bee colony algorithm. Int J Energy Environ Eng 2016;7:13–25. http://dx.doi.org/10.1007/s40095-015-0198-5.

[48] Lin P, Cheng S, Yeh W, Chen Z, Wu L. Parameters extraction of solar cell models using a modified simplified swarm optimization algorithm. Sol Energy 2017;144:594–603. http://dx.doi.org/10.1016/j.solener.2017.01.064.

[49] Alam DF, Yousri DA, Eteiba MB. Flower pollination algorithm based solar PV parameter estimation. Energy Convers Manage 2015;101:410–22. http://dx.doi.org/10.1016/j.enconman.2015.05.074.

[50] Ram JP, Babu TS, Dragicevic T, Rajasekar N. A new hybrid bee pollinator flower pollination algorithm for solar PV parameter estimation. Energy Convers Manage 2017;135:463–76. http://dx.doi.org/10.1016/j.enconman.2016.12.082.

[51] Askarzadeh A, Rezazadeh A. Artificial bee swarm optimization algorithm for parameters identification of solar cell models. Appl Energy 2013;102:943–9. http://dx.doi.org/10.1016/j.apenergy.2012.09.052.

[52] Askarzadeh A, Rezazadeh A. Extraction of maximum power point in solar cells using bird mating optimizer-based parameters identification approach. Sol Energy 2013;90:123–33. http://dx.doi.org/10.1016/j.solener.2013.01.010.
[53] Guo L, Meng Z, Sun Y, Wang L. Parameter identification and sensitivity analysis of solar cell models with cat swarm optimization algorithm. Energy Convers Manage 2016;108:520–8. http://dx.doi.org/10.1016/j.enconman.2015.11.041.
[54] Ma J, Ting TO, Man KL, Zhang N, Guan S-U, Wong PWH. Parameter estimation of photovoltaic models via cuckoo search. J Appl Math 2013;2013:1–8. http://dx.doi.org/10.1155/2013/362619.
[55] M. Louzazni, A. Craciunescu, E.H. Aroudam, A. Dumitrache. Identification of Solar Cell Parameters with Firefly Algorithm. In: 2015 2nd international conference on mathematics and computers in sciences and in industry; 2016. p. 7–12. doi: http://dx.doi.org/10.1109/MCSI.2015.37.
[56] Oliva D, Abd El Aziz M, Ella Hassanien A. Parameter estimation of photovoltaic cells using an improved chaotic whale optimization algorithm. Appl Energy 2017;200:141–54. http://dx.doi.org/10.1016/j.apenergy.2017.05.029.
[57] Sudhakar Babu T, Prasanth Ram J, Sangeetha K, Laudani A, Rajasekar N. Parameter extraction of two diode solar PV model using Fireworks algorithm. Sol Energy 2016;140:265–76. http://dx.doi.org/10.1016/j.solener.2016.10.044.
[58] El-Fergany A. Efficient tool to characterize photovoltaic generating systems using mine blast algorithm. Electr Power Compon Syst 2015;43:890–901. http://dx.doi.org/10.1080/15325008.2015.1014579.
[59] Ali EE, El-Hameed MA, El-Fergany AA, El-Arini MM. Parameter extraction of photovoltaic generating units using multi-verse optimizer. Sustainable Energy Technol Assess 2016;17:68–76. http://dx.doi.org/10.1016/j.seta.2016.08.004.
[60] Duan QY, Gupta VK, Sorooshian S. Shuffled complex evolution approach for effective and efficient global minimization. J Optim Theory Appl 1993;76:501–21. http://dx.doi.org/10.1007/bf00939380.
[61] Singer S, Nelder J. Nelder-mead algorithm. Scholarpedia 2009;4:2928. http://dx.doi.org/10.4249/scholarpedia.2928.
[62] Vrugt JA, Gupta HV, Bouten W, Sorooshian S. A shuffled complex evolution metropolis algorithm for optimization and uncertainty assessment of hydrologic model parameters. Water Resour Res 2003;39. http://dx.doi.org/10.1029/2002wr001642.
[63] Mariani VC, Coelho LdS. A hybrid shuffled complex evolution approach with pattern search for unconstrained optimization. Math Comput Simul 2011;81:1901–9. http://dx.doi.org/10.1016/j.matcom.2011.02.009.
[64] Mariani VC, Justi Luvizotto LG, Guerra FA, dos Santos Coelho L. A hybrid shuffled complex evolution approach based on differential evolution for unconstrained optimization. Appl Math Comput 2011;217:5822–9. http://dx.doi.org/10.1016/j.amc.2010.12.064.
[65] Zhao F, Zhang J, Zhang C, Wang J. An improved shuffled complex evolution algorithm with sequence mapping mechanism for job shop scheduling problems. Expert Syst Appl 2015;42:3953–66. http://dx.doi.org/10.1016/j.eswa.2015.01.007.
[66] Chu W, Gao X, Sorooshian S. A new evolutionary search strategy for global optimization of high-dimensional problems. Inf Sci 2011;181:4909–27. http://dx.doi.org/10.1016/j.ins.2011.06.024.
[67] Attivissimo F, Adamo F, Carullo A, Lanzolla AML, Spertino F, Vallan A. On the performance of the double-diode model in estimating the maximum power point for different photovoltaic technologies. Measurement 2013;46:3549–59. http://dx.doi.org/10.1016/j.measurement.2013.06.032.
[68] Ortiz-Conde A, Lugo-Munoz D, Garcia-Sanchez FJ. An explicit multiexponential model as an alternative to traditional solar cell models with series and shunt resistances. IEEE J Photovoltaics 2012;2:261–8. http://dx.doi.org/10.1109/JPHOTOV.2012.2190265.
[69] Nelson J. The physics of solar cells. London (United Kingdom): Imperial College Press; 2003.
[70] Chen Z, Wu L, Cheng S, Lin P, Wu Y, Lin W. Intelligent fault diagnosis of photovoltaic arrays based on optimized kernel extreme learning machine and I-V characteristics. Appl Energy 2017;204:912–31. http://dx.doi.org/10.1016/j.apenergy.2017.05.034.
[71] Chu W, Gao X, Sorooshian S. Handling boundary constraints for particle swarm optimization in high-dimensional search space. Inf Sci 2011;181:4569–81. http://dx.doi.org/10.1016/j.ins.2010.11.030.
[72] Fateen S-EK, Bonilla-Petriciolet A, Rangaiah GP. Evaluation of covariance matrix adaptation evolution strategy, shuffled complex evolution and firefly algorithms for phase stability, phase equilibrium and chemical equilibrium problems. Chem Eng Res Des 2012;90:2051–71. http://dx.doi.org/10.1016/j.cherd.2012.04.011.
[73] Tong NT, Pora W. A parameter extraction technique exploiting intrinsic properties of solar cells. Appl Energy 2016;176:104–15. http://dx.doi.org/10.1016/j.apenergy.2016.05.064.